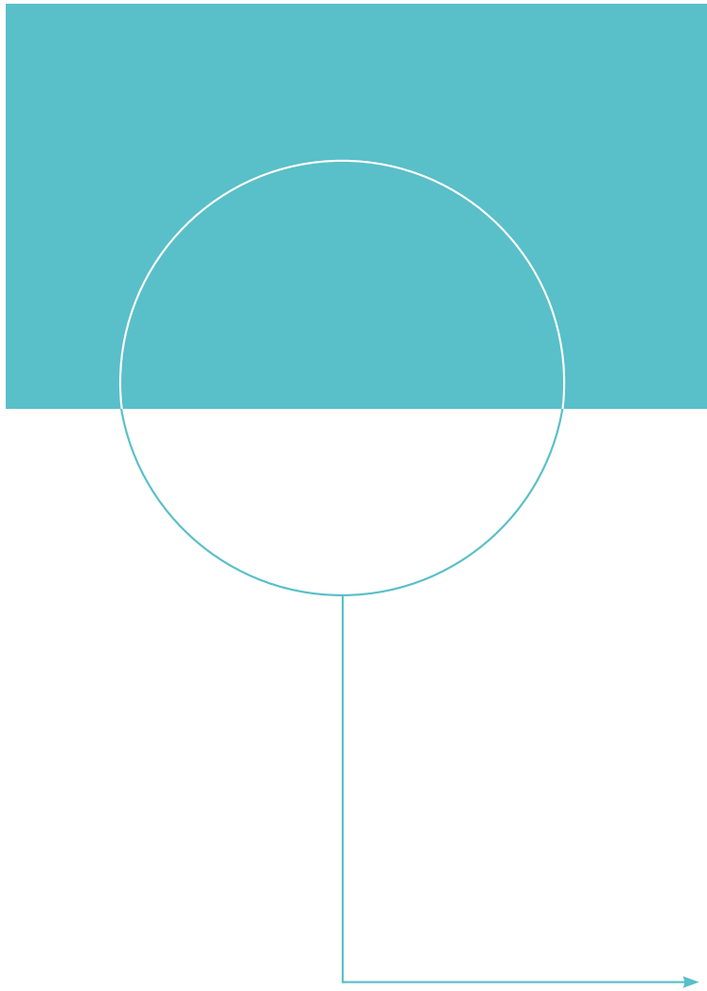

Master's thesis

2022

Jing Zhou

NTNU
Norwegian University of
Science and Technology
Faculty of Engineering
Department of Civil and Environmental Engineering

Jing Zhou

Development of a model and risk assessment for 1D steady seepage and transient contaminant advection-diffusion coupled process

June 2022

NTNU
Norwegian University of
Science and Technology

NTNU
Norwegian University of
Science and Technology

NTNU

Norwegian University of
Science and Technology

Development of a model and risk assessment for 1D steady seepage and transient contaminant advection-diffusion coupled process

Jing Zhou

Geotechnics and Geohazards
Submission date: June 2022
Supervisor: Yutao Pan

Norwegian University of Science and Technology
Department of Civil and Environmental Engineering

Preface

This is a Master's thesis in geotechnics at NTNU as part of the MSc in Geotechnics and Geohazards, which is supervised by Professor Yutao Pan at NTNU, and is the continuation of a series of works by Yutao Pan et al.

2022-06-11

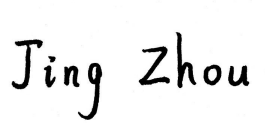

Jing Zhou

Acknowledgment

I would like to thank Professeor Yutao Pan and other helpful staff in NTNU during the writing of thesis. Without their support and patience, the thesis could not have been done.

J.Z.

Abstract

Cutoff walls are extensively applied as seepage and contaminant leakage obstruction structures. However, stochastic defects can exist within cutoff walls due to randomness in the construction of cutoff walls and faciliate the penetration of polluted groundwater through cutoff walls. To assess the contaminant leakage risk, definition and judge criterion for breakthrough time of cutoff walls with inhomogeneous Dirichlet boundary conditions are derived, and breakthrough time diagrams are plotted, which are based on the normalized analytical solution to one-dimensional linear steady seepage and transient contaminant advection-diffusion coupled process. The analytical solution also verifies its finite element method counterpart. For the purpose of assessing the contaminant leakage risk in a realistic way, a nonlinear model with nonconstant cross-sections along the penetration channel is obtained, which can be combined with planar and spacial models for cutoff walls with random defects, and a finite difference method algorithm for the nonlinear model is proposed, while an algorithm by Adomian decomposition method is also included for a trial.

Keywords: Construction errors; Cutoff wall; Contaminant leakage; Risk assessment; 1D seepage and contaminant advection-diffusion coupled process; Analytical solution; Breakthrough time; Nonlinear model; Adomian decomposition method

Contents

List of Figures

List of Tables

Chapter 1

Introduction

Cut-off walls widely serve as curtains to prevent groundwater from flowing into excavation pits and minimize drainage requirement for the pits (Groundwater Engineering Limited). They also function as waterproof structures to exclude contaminated water from non-polluted ground water (Figure 1.1) (U.S. EPA, 1978; Sembenelli and Sembenelli, 1999; Croce and Modoni, 2007).

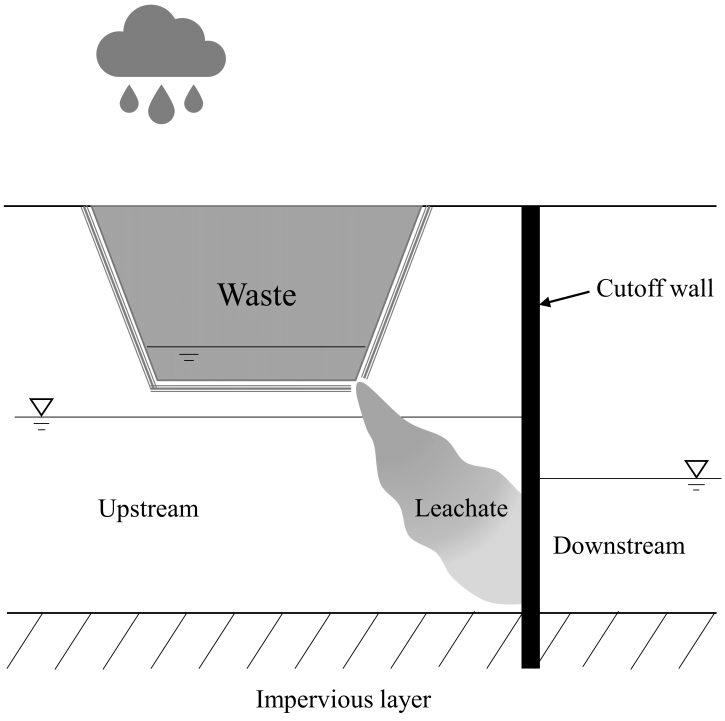

Figure 1.1: Cutoff wall to prevent waste leachate from flowing into non-contaminated groundwater

However, construction errors can happen due to imperfection and randomness in construction

technology and quality (Wu et al., 2015a,b; Tan and Lu, 2017), which can lead to existence of untreated zones, i.e. windows through which groundwater can seep directly (Figure 1.2). It can result in an increase in flow rate around the untreated zones (Amos et al., 2020), and in serious situations bring about hazardous consequences, such as ground collapse, building tilting, land subsidence and breach of pipelines, etc (Pujades et al., 2012, 2016; Conway, 2016; Liu et al., 2018).

As the concern for environmental protection has been publicly raised, to minimize the potential threat to environmental and public health due to contaminant leakage in the ever-increasing dump sites, it is essential to investigate the contaminant leakage risk for imperfect cut-off walls by developping reasonable models.

The leakage risk for 1D linear steady seepage and transient contaminant advection-diffusion coupled process is assessed by breakthrough time, and a nonlinear model for the steady seepage and transient contaminant advection-diffusion coupled process is developped, of which the cross-sectional area is nonconstant. The FDM algorithm as a numerical method is given and a trial on the ADM method is included as well.

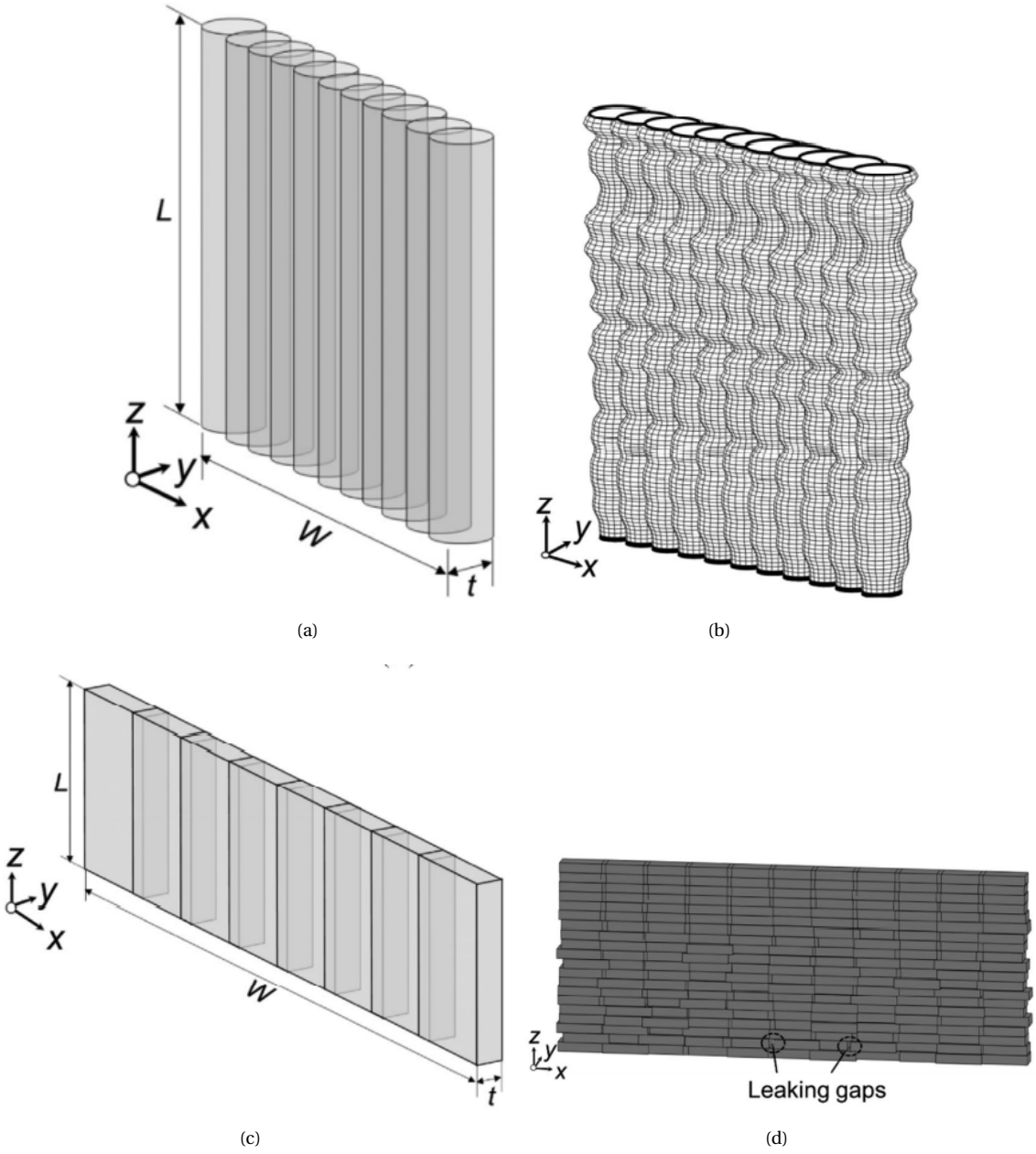

Figure 1.2: Two widely used cutoff walls : (a) jet-grouted cutoff wall (perfect); (b) jet-grouted cutoff wall (with defects); (c) diaphragm wall (perfect); (d) diaphragm wall (with defects) (Pan et al., 2021)

Chapter 2

Literature review

Within the scope of cutoff walls, cases for leakage resulted accidents, the parameters for construction defects, currently applied methods to assess the leakage risk and researches for contaminant leakage problems are collected and reviewed in this chapter to give an overall impression on the detrimental consequences of seepage and contaminant leakage in cutoff walls and emphasize on the necessity to perform the risk assessment for the seepage and contaminant leakage problems.

2.1 Cases for hazards due to leakage in cutoff walls

Cases for the accidents in dams, excavation pits and landfills due to the leakage are reviewed in this section.

2.1.1 Cases for hazards due to leakage in dams

Three sinkholes were found to be at the top of the Unmun Dam in Korea and the leakage was augmented as the precipitation increased (Lee et al., 2005). By back analysis, Sembenelli (2016) verified piping to be blamed for the leakage under a sandfill dam, which led to its failure. The Fountain of Gazelles dam in Biskra, Algeria suffered from leakage in its right part according to Ratiat et al. (2020), which put the dam in a dangerous situation. The detrimental consequences caused by seepage in dams were discussed by Adamo et al. (2020), in which sloughing, piping, erosion and instability can result from the daylighting of the flow at the downstream surface of dams and be intensified by leakage due to earthquakes or uneven settlement of dams.

2.1.2 Cases for hazards due to leakage in excavations

It was reported by Shin et al. (2006) that slurry flowed in the subway tunnel under construction in Seoul, resulting in the collapse of the tunnel in downtown areas. According to Tan and Lu (2017), in a deep excavation of a subway station in Shanghai, an outbreak of underground water happened unexpectedly and submerged the pit, causing the ground and buildings in the vinicity to fall steeply, which was due to the carelessness on the previous small leakage and the imperfection in the waterproof structure components (Figure 2.1(a)). A serious water leakage incident occured during the construction of the tunnels LUO09 in Kaohsiung, which was due to the piping in the tunnel as stated by Cheng et al. (2019) and can be seen in 2.1(b). The width of the actual overlapped zones of jet grouted mass is less than the design value due to the inclination of the jet grouted columns, which spawned leakage susceptible zones.

(a) (b)

Figure 2.1: In-situ photos for excavation leakage accidents: (a) pit corner in the northwest on July 7, 2013 in a subway station in Shanghai (Tan and Lu, 2017); (b) north and south cave-ins in tunnels LUO09 in Kaohsiung (Cheng et al., 2019)

2.1.3 Cases for hazards due to contaminant leakage in landfills

The yearly leakage from the Ano Liosia landfill in Greece resulted in the undergound water pollution, makng it not drinkable and not safe for agriculture, which was based on Fatta et al. (1999). Abu-Rukah and Al-Kofahi (2001) reported that in northern Jordan, leachate from the El-Akader dump landfills caused a significant harm to the adjacent underground water system. 43 cases of contaminants of emerging concern (CEC) in 10 regions in China were reviewed by Qi et al. (2018), of which the distribution map can be seen in Figure 2.2, and the awareness that adjacent aquifers be protected from the leachate were stated.

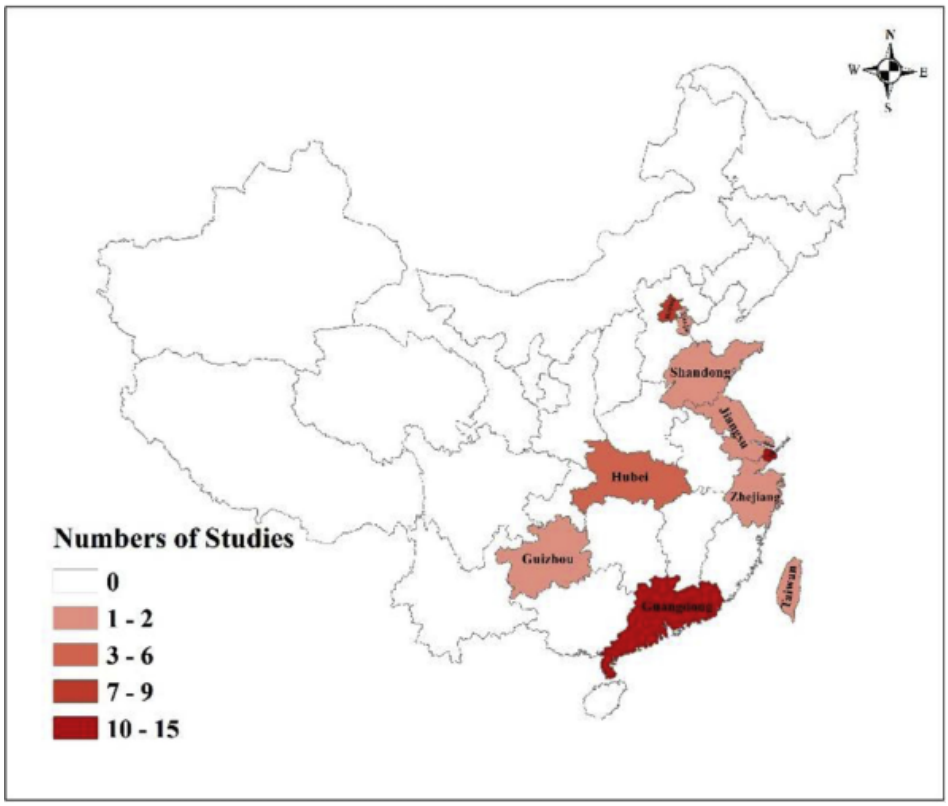

Figure 2.2: Distribution of cases with CECs in landfill leakage in China (Qi et al., 2018)

2.2 Construction errors in cutoff walls

The major causes and relevant statistical parameters for the construction errors in JGCOW are discussed in this section.

2.2.1 Construction errors in JGCOW

The geometric imperfection in JGCOW can be characterized by certain random parameters. As can be seen in Table 2.1 and Figure 2.3, there are two types of geometric imperfections in JGCOW, i.e. orientation imperfection and diameter imperfection of jet-grouted columns, of which the orientation imperfection is characterized by the azimuth angle α and inclination angle β (Croce and Modoni, 2007; Flora et al., 2012; Modoni et al., 2016; Pan et al., 2017). The azimuth angle is assumed to be uniformly distributed within $[0,\pi]$, since a jet-grouting machines can tilt its mast in any direction during the jet-grouting(Pan et al., 2019a).

Some statistical data for the diameter D and inclination angle β of JGCOW in several types of soils are collected in Table 2.2, where COV(D) is the coefficient of variation of column diameter

Table 2.1: Random parameters representing construction errors in JGCOW

Orientation imperfection [°]		**Diameter variation [m]**
Azimuth α	Inclination β	Diameter D

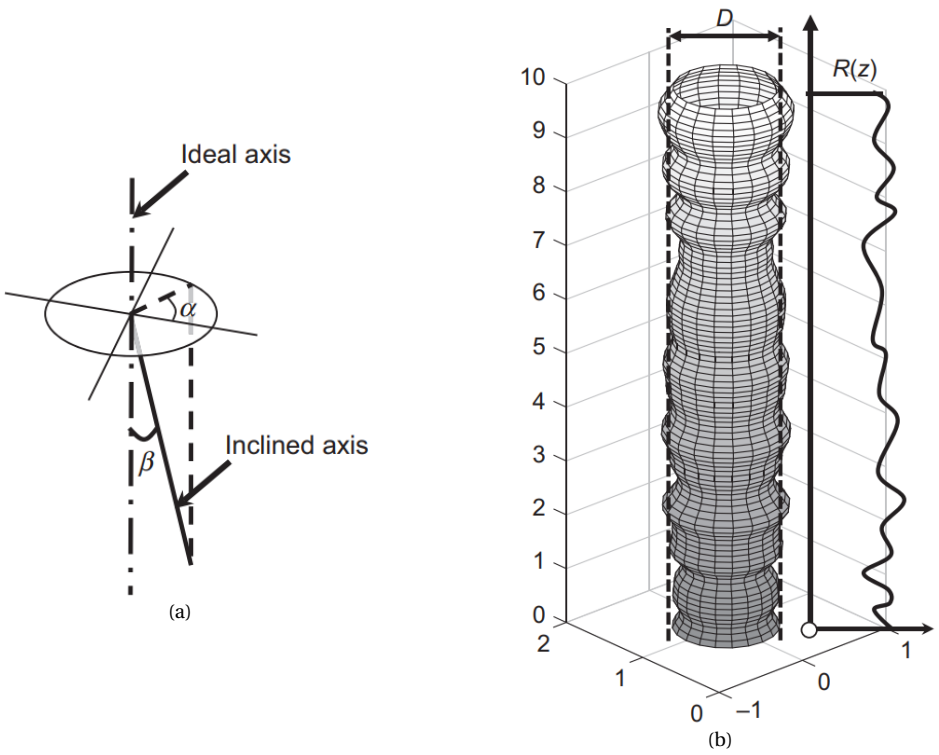

Figure 2.3: Two categories of geometric imperfections in JGCOW: (a) azimuth α and inclination angle β; (b) variation of column diameter D (Pan et al., 2019a)

and S.D.(β) is the standard deviation of column inclination.

Table 2.2: Statistical data for the geometric randomness in JGCOW (Pan et al., 2021)

No.	**Type of natural soil**	**Average diameter [m]**	**COV(D)**	**S.D.(β)**	**Details**	**References**
1	Clay-silt	-	0.02-0.05	-	-	Croce et al. (2004)
	Sand		0.02-0.10			
	Gravel		0.05-0.25			
2	Sandy clay	1.1	0.06-0.09	-	From field diameter data at different depths, horizontal column	De Wit et al. (2007)
3	Silty sand	0.71-1.11	0.06	0.07°	Vertical columns at Vesuvius site (0.07° was from Isola Serafini site)	Croce and Modoni (2007)
	Sandy gravel	1.06-1.20	0.19		Vertical columns at Polcevera site	
4	Silty sand	2.5	-	0.16°	Vertical columns at Barcelona site	Eramo et al. (2012)
5	Sandy clay	0.38	0.13	-	Vertical column with lower water content	Arroyo et al. (2012)
		0.48		-	Vertical column with lower water content	
		0.75	0.17	0.17°	(Sub) Horizontal column	

2.2.2 Construction errors in diaphram wall

According to Castaldo et al. (2018), the inclination angle ϕ, the excavation height H and the overlapping dimension d between two adjoined diaphram walls are the statistical parameters for the leakage estimation, which are illustrated in Table 2.3 and Figure 2.4. The inclination angle ϕ follows the truncated Gaussian distribution in Equation 2.1:

$$\phi \sim N(\mu_\phi, \sigma_\phi, -\left|\phi(h_{control})\right|, +\left|\phi(h_{control})\right|), \tag{2.1}$$

where μ_ϕ is the mean value, σ_ϕ is the standard deviation and $-\left|\phi(h_{control})\right|$ and $+\left|\phi(h_{control})\right|$) are the lower and upper bounds of the inclination angle ϕ.

Table 2.3: Random parameters representing construction errors in adjoining diaphram walls

Inclination angle [°]	**Excavation height [m]**	**Overlapping dimension [m]**
ϕ	H	d

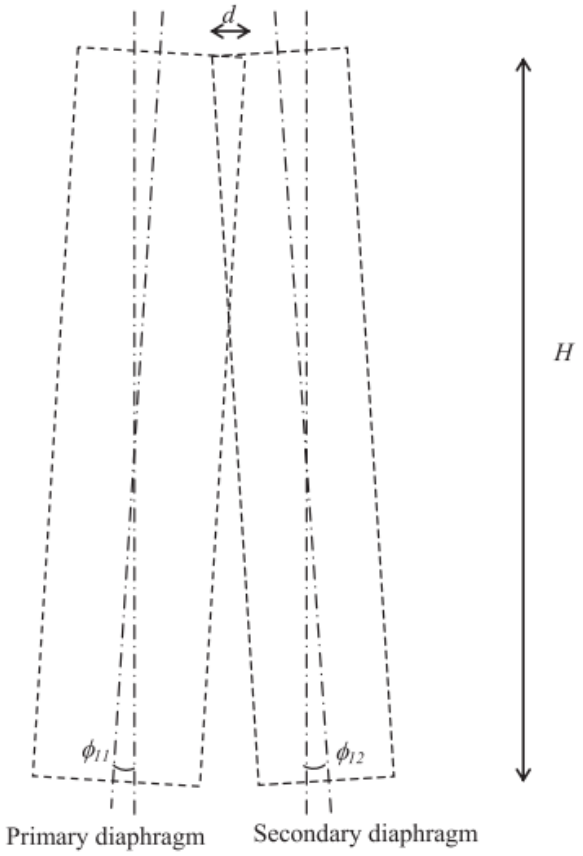

Figure 2.4: Two inclined adjoining diaphram walls (Castaldo et al., 2018)

2.3 Leakage risk assessment

Multi researches have been done to evaluate the leakage risk in cutoff walls and the methods are classified into analytical, experimental, numerical and TDA methods in general.

2.3.1 Analytical methods

With the steady-state flux equations, Devlin and Parker (1996) stated that there are a best range of hydraulic conductivities for cutoff wall material in which the outward diffusive flux can be countered balanced by an inward dispersive and advective flux.

Wang et al. (2021) developed a theoretical model, which was the combination of the statistical 3D model from field experiments and a simple seepage model, to assess the leakage through the windows in JGCOW, which was justified by program simulation and in-situ inspection. Based on the theoretical equations, the parametric design of JGCOW can be performed and the amount of leakage can be estimated.

2.3.2 Experimental methods

Liu et al. (2019) assessed the utility of the distributed optical fiber temperature measurement system to monitor the leakage in diaphragm barriers by experiments.

A mini-scaled landfill cutoff wall model made of polyvinyl alcohol-bentonite-fly ash-cement (PBFC) was used to simulate the accurate deformation in the cutoff wall experimentally by Dai et al. (2020) for leakage control. The results of the numerical simulation by ANSYS were compared with the measured data from the test, and the comparison showed difference.

2.3.3 Numerical methods

Castaldo et al. (2018) assessed the leakage probability in reinforced concrete retaining walls due to construction imperfections and trench instability. By Bayesian updating, suggestions on the effectiveness and importance of the monitoring phase for the reduction of the failure probability are given.

In-situ alignment data about vertical and inclined JGCOW were collected to model the 3D JGCOW with the statistical method by Cheng et al. (2020), in which the non-overlapped areas were inspected.

Hwang et al. (2019) gave suggestions on the specifications for the waterproof walls with bottom and vertical parts by program simulation for the seepage-advection-dispersion process.

Hekmatzadeh et al. (2019) innovated the combination of the concept of random field theory with the lattice Boltzmann method to simulate a two-dimensional advection-dispersion process in a probablistic way, in which the chemical reaction is also considered.

2.3.4 Three-dimensional Discretized Algorithm

Pan et al. (2017, 2019a) used a three-dimensional discretized algorithm (TDA) to simulate the construction errors in JGCOW with one-dimensional steady state seepage and proposed dimensionless design charts and design procedures for engineers to determine the parameters for excavation with acceptable flow rate and the least treatment volume.

It was further shown by Pan et al. (2019b) that in the JGCOW case the TDA has a strong connection with random finite element method (RFEM) and much lower computational cost when compared with 3D RFEM. An analogical research for diaphragm walls is conducted by Pan and Fu (2019).

Moreover, Pan et al. (2021) extended the TDA to quantitatively estimate the transient-state discharge rate through defective cut-off walls.

2.4 Contaminant leakage in cutoff walls

The harmful substances in the waste landfills and other poisonous mass bodies can be carried by the water from rainfall or underground flow to adjoining unpolluted zones, which can be impeded by watertight structures ,such as JGCOW and slurry trench cutoff walls. However, since defects might be within the waterproof structures, it is necessary to evaluate the risk and per-

form the risk assessment for the contaminant leakage.

Studies about the leachate from dump sites to date have been focusing on the application of analytical and numerical methods, the cutoff wall material and field test and case study, which shall be reviewed later.

2.4.1 Works done

A 2D analytical method was established by Ding et al. (2020) to explain the migration of organic pollutants through an underground system with a cutoff barrier, while another 2D analytical model was introduced by Peng et al. (2020) to study the transient diffusion behavior of the contaminant from an organic pollutant source in an aquifer-CGCW system and the service effectiveness of a CGCW in a comprehensive way.

As for numerical simulation, Inazumi et al. (2009) and Shishido and Inazumi (2019) evaluated the environmental feasibility, which is the prevention of polluted water migration, by comparing a 3D arrangement and distribution of the hydraulic conductivity of the joint sections in the steel pipe sheet pipe (SPSP) cutoff wall with another part using the equivalent hydraulic conductivity. Zhan et al. (2013) used a finite difference model based on a trash landfill to study the time for the COD contaminant to go through the cutoff wall under different paramenters and materials. Inazumi et al. (2017) quantitatively assessed the pervasion of the harmful leachate in landfills near the coast where the watertightness of the waterproof side walls is harmed as the walls perished.

Experiments were carried out by Rowe and Abdelatty (2013) to inspect the movement of pollutants through a circular opening in a geomembrane connected directly to a geosynthetic clay liner (GCL) and nearby silty sand. Koh (2018) suggested that the underground cement cutoff wall can effectively stop the transport of leachate from rubbish landfill by visual examination and experiments. Naveen et al. (2018) conducted a number of batch and column tests, of which the results were put into the fuidyn-POLLUSOL model to simulate the movement of foul water to adjacent water bodies. Beneficial experience can be learned from Feng et al. (2020), in which an integrated method was taken to assess and restrain the migration of harmful leachate from

the MSW landfill to the underground project in the vicinity.

Soil-bentonite (SB) cutoff walls are proven to be effective in the containment of contaminants. Wang et al. (2016) conducted column and batch experiments to look into the adhesion and migration of Pb(II) in soil-bentonite modified by Chinese loess, which is a effective absorbent to collect heavy metals on the surface of the loess. Environmental hazards due to the previous landfills and areas exposed to pollution are considered by Koda and Osinski (2017) by in-situ and laboratory hydraulic conductivity tests for vertical SB cutoff walls and the remediations for a landfill in Poland are included. The in-situ data in the backfill of an experimental soil-bentonite cutoff wall was collected by Evans and Ruffing (2017) to understand its behavior in a more thorough manner. Adsoprtion data collected formerly and numerical migration stimulations were utilized to study the performance of the zeolite-enhanced soil-bentonite cutoff wall regarding the prevention of the transport of potassium (K) and zinc (Zn) by Hong et al. (2017). Chemical compatibility of SB barriers under the influence of compound pollutants is researched using the model backfills according to Xu et al. (2019). Du et al. (2015) examined the hydraulic conductivity and capability of compression of clayey soil/Ca-bentonite barriers in the context of lead contamination, which was also the pollution source in the laboratory work on the properties of sand/sodium hexametaphosphate-amended bentonite (SHMP-SB) backfills in cutoff barriers by Fu et al. (2021).

2.4.2 Limitation

Although many works have been done about the pollutants migration, the current methods are mainly deterministic, while in reality the orientation and deformation of the waterproof barriers and the randomness due to construction and geological conditions shall be emphasized.

The aim of the thesis is to develop a risk assessment criterion and a nonlinear model to evaluate the transport of contaminant mass in cutoff walls with stochastic construction errors, which are simulated by models for cutoff walls with random construction defects. With the results of the coupled model, it is hopeful to give useful suggestions for the contaminant leakage problems in the cutoff walls.

Chapter 3

Methodology and derivations

The TDA method by Pan et al. (2017, 2019a, 2021) is reviewd in the chapter, which is a numerical method to simulate the anamolistic apertures in the JGCOW due to randomness in the jetgrouting of the JGCOW. The leakage risk is assessed by coupling with the discretized cross-sectional areas and solving the 1D diffusion or advection-diffusion governing equations. The numerical methods to solve the 1D governing equations are the FDM method by Pan et al. (2021) and the FEM method by Schirén (2018).

As for the works by the thesis, the detailed derivation of the analytical solution to the 1D linear steady seepage and transient contaminant advection-diffusion coupled equation with inhomogeneous Dirichlet boundary conditions is given, which is obtained by the method of separation of variables (Brown and Churchill, 1993; Mojtabi and Deville, 2015) and a change of variable technique (Guerrero et al., 2009), and the result agrees with the 1D solution in test case 1 in Guerrero et al. (2009), which is obtained by integral transform technique. With the analogical solution, the hydraulic gradient for the 1D linear transient seepage process is proved to be Jacobi theta equation, as well as the contaminant flux for the 1D linear transient contaminant diffusion process derived later.

It is done in the thesis that the time and contaminant flux are normalized to simplify the equations and faciliate the plotting of relevant diagrams. A different definition to understand the Péclet number is given which is based on the characteristic time for the normalization of time. The definition of breakthrough time for 1D linear steady seepage and transient contaminant

advection-diffusion coupled process with inhomogenous boundary conditions is given, and the judge criteria for breakthrough time with different ranges of Péclet number is derived.

The contribution by the thesis also includes a model which governs the 1D nonlinear steady seepage and transient contaminant advection-diffusion coupled process is derived, where the cross-sectional area along the path is noncontant, and the boundary conditions for the seepage process are inhomogeneous Dirichlet boundary conditions. A FDM algorithm to solve the governing equation is given and the ADM method is applied to give a trial to the governing equation.

3.1 TDA method

To assess the seepage leakage or the contaminant leakage risk due to stochastic construction defects in JGCOW, the combination of the TDA 3D model and algorithms to solve the seepage or contaminant advection-diffusion governing equation is necessary.

3.1.1 TDA 3D model

As a numerical method, the 3D model shall give the discretized cross-sectional areas in each groundwater channel in the JGCOW and provide the characteristic waterproofness for the JGCOW with or without penetration.

3.1.1.1 Statistical characteristics

As previously mentioned, the parameters for geometric imperfections for JGCOW consist of the azimuth angle α, inclination angle β and diameter of columns D, where α and β are independent from each other. The inclination angle β is normally distributed with the mean value being zero (Croce and Modoni, 2007; Arroyo et al., 2012). The orientation parameters, i.e. the azimuth angle α and inclination angle β are independently identically distribution (IID) parameters (Modoni et al., 2016).

To state the correlation among the azimuth angle α and inclination angle β for adjoining columns, Pan et al. (2019a) suggested a random field with autocorrelation structure other than a collec-

tion of IID random numbers to supplement the earlier reaserches where only the mean value and coefficient of variation (COV) were considered (Croce and Modoni, 2007; Modoni et al., 2016).

The scale of fluctuation (SOF) of orientation parameters is considered as well, which describes the correlation among close-by columns, and is approximately defined as the largest distance between two points which have a certain degree of similarity. The 2D random field is defined by Equation 3.1 (Pan et al., 2019a)

$$\rho\left(\Delta x, \Delta y\right) = e^{-\pi\left[\left(\frac{\Delta x}{\delta x}\right)^2 + \left(\frac{\Delta y}{\delta y}\right)^2\right]}, \tag{3.1}$$

where Δx and Δy are the distances between two points and δx and δy are the SOFs in x and y directions respectively.

The relations between column diameter D and jet-grouting parameters along with other soil properties have been researched (Modoni et al., 2006; Ho, 2007; Flora et al., 2013; Shen et al., 2013), and the diameter D should vary greatly along each column as the natural soils are stratified, making columns calabash shaped (Figure 2.3(b))(Pan et al., 2019a).

As the horizontal SOFs of soil properties are usually considerably greater than the vertical ones (Phoon and Kulhawy, 1999), it is reasonable to regard the randomness in column diameter D as the result of the stratification in soil profiles, which can be simulated by a stochastic process where the vertical SOF is applied (Pan et al., 2019a).

3.1.1.2 3D model for the evaluation of geometric errors

Pan et al. (2019a) developed a 3D model, which adopted thousands of Monte Carlo simulations to evaluate the construction errors in JGCOW to consider the randomness of orientation and diameter of jet-grouting columns concurrently (Figure 3.1).

It can be seen in Figure 3.2(a) that the JGCOW is discretised into the same sized small cubes with eight nodes on the vertexes of each cube. The horizontal planes (x-y plane) and vertical planes (x-z) are called "layers" and "slices" respectively, where "slices" along the y-direction are

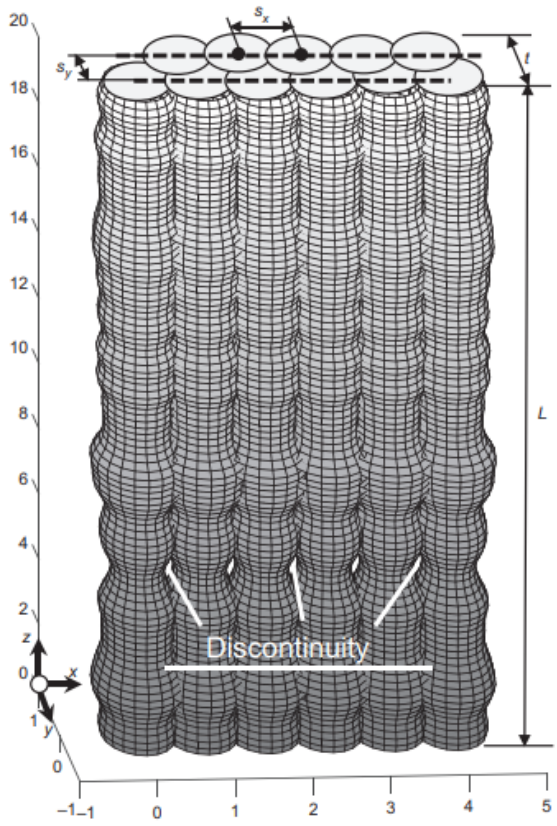

Figure 3.1: One typical realisation of JGCOW with construction errors (Pan et al., 2019a)

parallel to the JGCOW plane. The treated area, which is the grey part in Figure 3.2(b), is used to examine whether there are any nodes located there. If so, the nodes will be noted as "treated", otherwise "untreated".

The groundwater is assumed to flow through the slices perpendicularly, and the cross-sectional areas of the untreated zone in each slice are calculated by counting the number of nodes in untreated zones. The area is proportional to the number of untreated nodes, and one node should represent an area which is the area for one surface of a small cube (Figure 3.2(c)).

Each slice in the model will be integrated to determine whether the JGCOW is penetrated by the untreated zones. The JGCOW is thought to be penetrated a window, i.e. an continuous untreated zone if any two arbitrary consequent slices are found to be overlapped (Figure 3.2(d)), and penetration only happens in the third scenario.

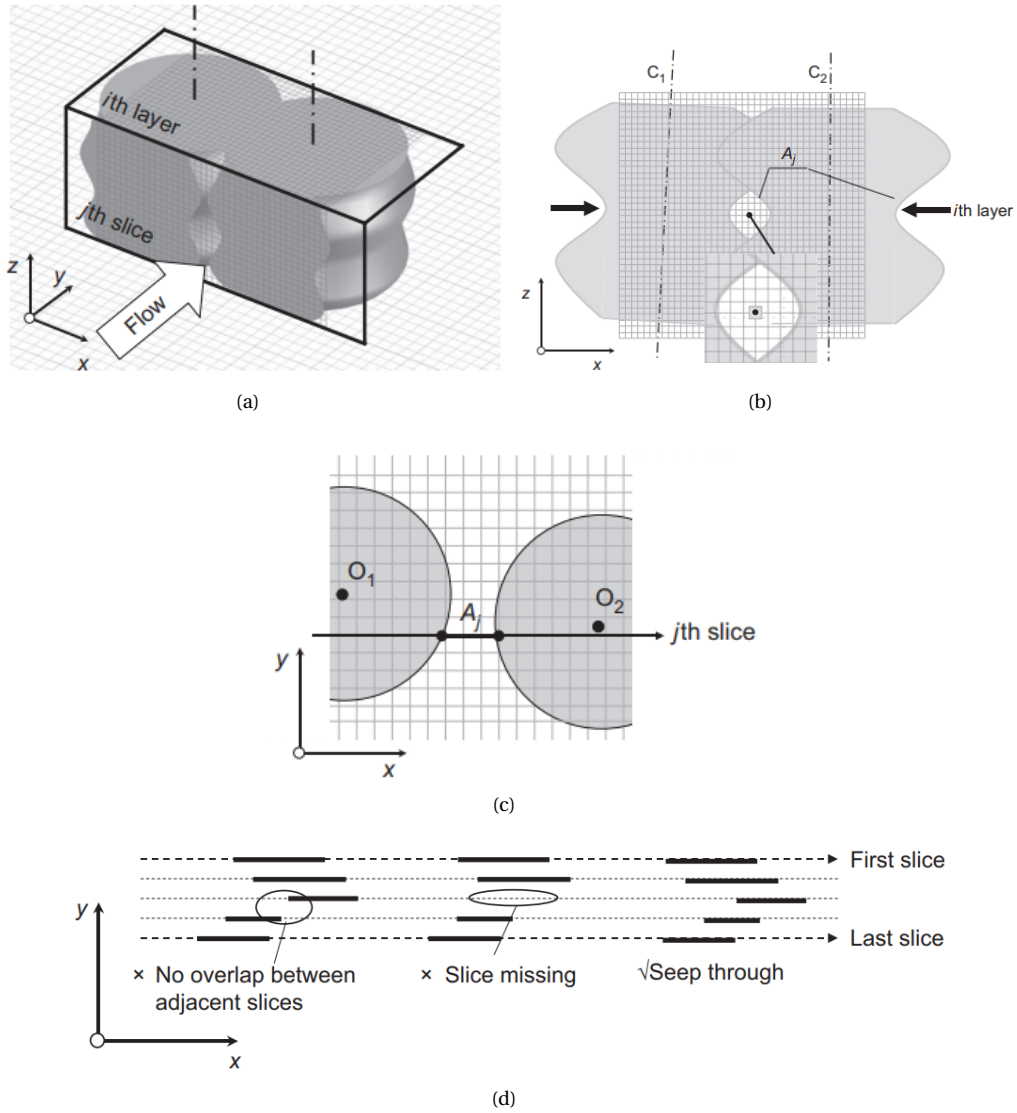

Figure 3.2: Discretization of JGCOW: (a) 3D view; (b) vertical plane view at the i-th layer; (c) horizontal plane view at the j-th layer; (d) overlapping situations for JGCOW (Pan et al., 2019a)

To give an direct impression, the algorithm in flow chart can be seen in Figure 3.3.

3.1.1.3 Estimation of minimum thickness

The minimum thickness represents the waterproof capacity of the JGCOW when the wall is continuous (Croce and Modoni, 2007). By determining the number of treated nodes along the y-direction in each layer, the minimum thickness is obtained which is the minimum value in all layers (Figure 3.4) (Pan et al., 2019a).

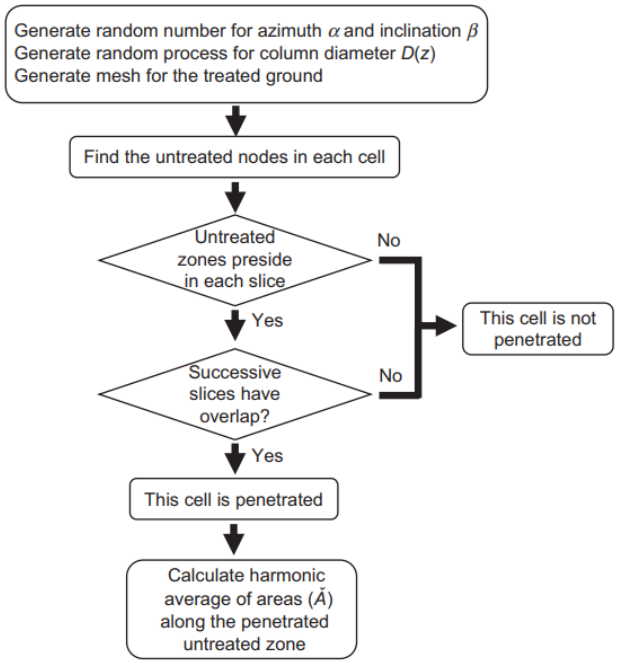

Figure 3.3: Flowchart for TDA (Pan et al., 2019a)

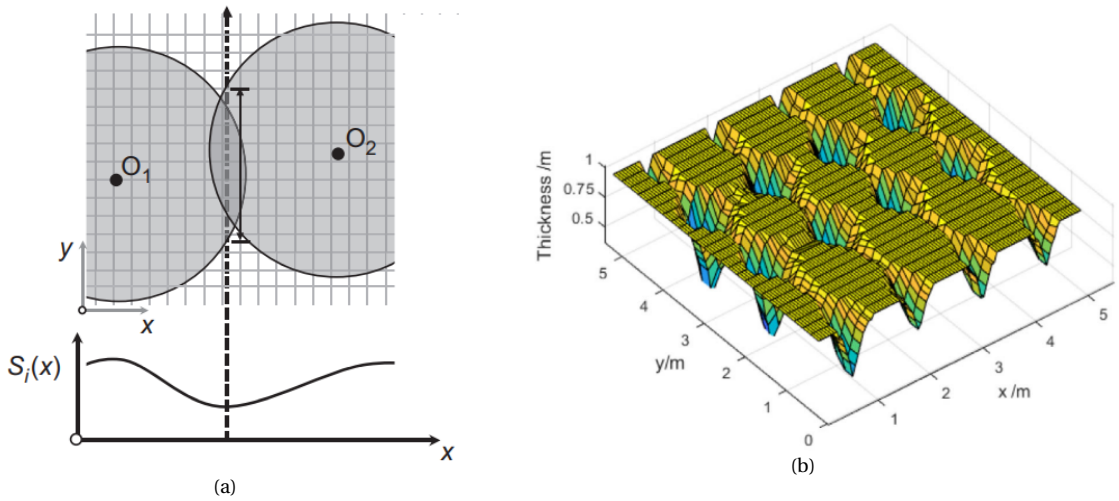

Figure 3.4: Illustrations for representative thickness: (a) thickness of the wall by scanning the number of treated nodes (Pan et al., 2019a); (b) example of wall thickness distribution (Pan et al., 2021)

3.1.2 TDA for steady seepage

Pan et al. (2019a) noted that the minimum thickness is zero once the JGCOW is penetrated. Therefore, it is not reasonable to evaluate the water-proofness of penetrated JGCOWs by the minimum thickness. To give an appropriate solution, the sizes of the windows along with the flow rate are selected to be appropriate to assess the water-proofness of JGCOW (Modoni et al.,

2016; Pan et al., 2017).

The steady state flow through the JGCOW is considered mainly as a 1D process (Modoni et al., 2016) and is governed by Darcy's law (Pan et al., 2017)

$$Q = ki\left(y\right)A\left(y\right), \tag{3.2}$$

where Q is the flow rate of groundwater through the JGCOW, k is the coefficient of permeability for the untreated soil, $i\left(y\right) = \frac{dh}{dy}$ is the hydraulic gradient through a slice with coordinate y, h is water head and $A\left(y\right)$ is the stochastically generated untreated cross-sectional area in the slice with coordinate y for one continuous window.

Since $i\left(y\right) = \frac{dh}{dy}$, Equation 3.2 becomes

$$\frac{Q}{A\left(y\right)}dy = kdh. \tag{3.3}$$

To be in accordance with the principle of flow continuity, the inflow and outflow through the window in each slice shall not change. By integrating, Equation 3.3 is

$$\int_{T_{wall}}^{0} \frac{Q}{A\left(y\right)}dy = \int_{\Delta H}^{0} kdh, \tag{3.4}$$

where T_{wall} is the nominal thickness of the JGCOW and ΔH is the constant water head difference between the two sides of the JGCOW.

Therefore, Equation 3.4 can be expressed as

$$Q = \frac{k\Delta H}{T_{wall}}\tilde{A}\left(T_{wall}\right), \tag{3.5}$$

where $\tilde{A}\left(T_{wall}\right) = \frac{1}{\frac{1}{T_{wall}}\int_{0}^{T_{wall}} \frac{1}{A(y)}dy}$ is the harmonic average area along the seepage path.

To calculate $\tilde{A}\left(T_{wall}\right)$ numerically, the discritized harmonic average area is shown as

$$\tilde{A}\left(T_{wall}\right) = \frac{1}{\frac{1}{n}\sum_{j=1}^{n}\frac{1}{A_j}}, \tag{3.6}$$

where A_j is the cross-sectional area of the flow way at the jth slice when the JGCOW is divided into n slices equally.

To faciliate the application of flow rate, its normalized form is defined as (Modoni et al., 2016)

$$\Omega = \frac{QT_{wall}}{k\Delta H A_w} = \frac{\tilde{A}(T_{wall})}{A_w}, \tag{3.7}$$

where A_w is the area of JGCOW.

By summing up the flow rates through the windows between each adjoining columns, the total flow rate for the whole JGCOW shall be calculated (Pan et al., 2019a).

3.1.3 TDA for transient seepage and diffusion process

The Laplace's equation, which is also the Fick-Jacobs diffusion equation, decribes the general transient seepage or diffusion process, which is shown in Equation 3.8 (Pan et al., 2021):

$$A\frac{\partial \phi}{\partial t} = \frac{\partial}{\partial y}\left(DA\frac{\partial \phi}{\partial y}\right), \tag{3.8}$$

where t is the time coordinate for the process, $\phi(y,t)$ is the potential for the process, which can have different definitions in various scopes, and D is the coefficient of diffusivity.

Although in reality Equation 3.8 is not sufficient to describe the seepage process since the diffusion coefficient D can be of great difference between treated and untreated soils, for simplicity here D is regarded as the constant coefficient of the consolidation for the seepage process, which has relations to the permeability coefficient k, constrained modulus m_v, and bulk unit weight of water γ_w. Properties of D in seepage along with its other definitions and properties in heat transfer can be seen in Table 3.1.

The coefficient of volume compressibility m_v is defined in Equation 3.9 according to Tyagi et al. (2017):

$$m_v = \frac{(1+\nu') \times (1-2\nu')}{E' \times (1-\nu')}, \tag{3.9}$$

where E' is the effective Young's modulus, ν' is the Possison's ratio of the treated soil (Lambe and

Table 3.1: Parameters in Laplace's equation for two engineering scopes (Pan et al., 2021)

Parameter	Symbol	Seepage	Heat transfer
State value	ϕ	Water head unit: m	Temperature unit: K
Coefficient of diffusivity unit: m^2/s	D	$D_w = \frac{k}{\gamma_w m_v}$ k- coefficient of permeability (unit: m/s); γ_w- unit weight of water (unit: kN/m^3); m_v - compressibility coefficient (unit: m^2/kN)	$D_T = \frac{k}{\rho c}$ k- thermal conductivity (unit: W/m/K); ρ- density (unit: kg/m^3); c- specific heat capacity (unit: J/kg/K)
Discharge rate	q	unit: m^3/s	unit: W

Whitman, 1969).

To study the groundwater flow, $\phi(y,t)$ is regarded as the water head in the following procedure, although the results are applicable for heat transportation as well.

Since the cross-sectional area $A(y)$ is random and continuous, it is possible to solve Equation 3.8 only numerically, and a FDM alogirthm is derived by Pan et al. (2021). Equation 3.8 is thus rewritten as

$$\frac{A}{D}\frac{\partial \phi}{\partial t} = \frac{dA}{dy}\frac{\partial \phi}{\partial y} + A\frac{\partial^2 \phi}{\partial y^2}. \tag{3.10}$$

The time and space are discretized (Figure 3.5), and the space is segmented in accordance to the slices. Therefore, by difference methods the differential parts in Equation (3.10) can be substituted by

$$\begin{cases} \dfrac{\partial \phi}{\partial t} = \dfrac{\phi_j^{m+1} - \phi_j^m}{\Delta t} \\ \dfrac{dA}{dy} = \dfrac{A_{j+1} - A_{j-1}}{2\Delta y} \\ \dfrac{\partial \phi}{\partial y} = \dfrac{\phi_{j+1}^m - \phi_{j-1}^m}{2\Delta y} \\ \dfrac{\partial^2 \phi}{\partial y^2} = \dfrac{\phi_{j+1}^m - 2\phi_j^m + \phi_{j-1}^m}{\Delta y^2} \end{cases}, \tag{3.11}$$

and Equation 3.10 is reformed into Equation 3.12:

$$\frac{A_j}{D}\frac{\phi_j^{m+1} - \phi_j^m}{\Delta t} = \frac{A_{j+1} - A_{j-1}}{2\Delta y}\frac{\phi_{j+1}^m - \phi_{j-1}^m}{2\Delta y} + A_j\frac{\phi_{j+1}^m - 2\phi_j^m + \phi_{j-1}^m}{\Delta y^2}, \tag{3.12}$$

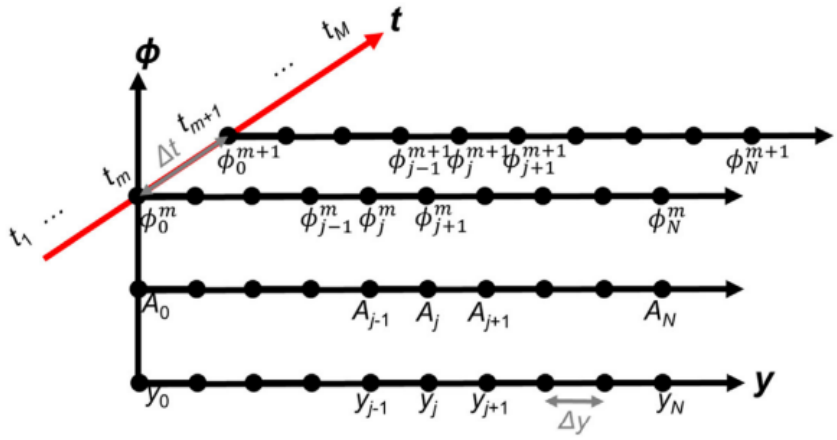

Figure 3.5: 1D Finite difference method (FDM) model with cross-sectional area varying in space (Pan et al., 2021)

where A_j is the cross sectional area at the jth slice (Figure 3.6), ϕ_j^m is the water head at the jth slice and mth time node, $\Delta t = \frac{T}{M}$ is the time interval, where T is the total time for the transient flow process and M is the number of time intervals, $\Delta y = \frac{T_{wall}}{N}$ is the length of the segment in space, where N is the number of the segments in the y direction.

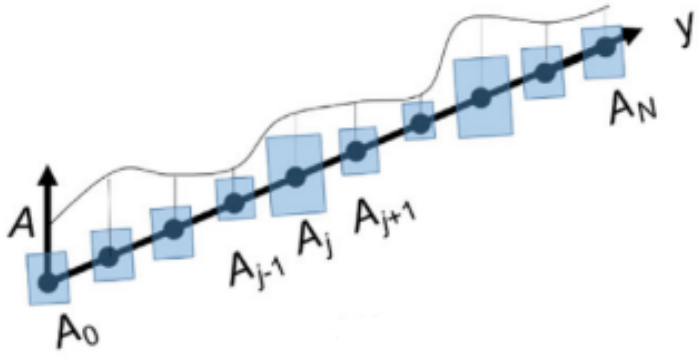

Figure 3.6: Untreated cross-sectional area along the seepage path (Pan et al., 2021)

By rearranging Equation 3.12, Equation 3.13 is derived:

$$\phi_j^{m+1} = \phi_j^m + \frac{D\Delta t}{\Delta y^2}\left(\frac{A_{j-1}+4A_j-A_{j+1}}{4A_j}\phi_{j-1}^m - 2\phi_j^m + \frac{-A_{j-1}+4A_j+A_{j+1}}{4A_j}\phi_{j+1}^m\right). \tag{3.13}$$

When $t = t_m$, $(N+1)$ unknowns and $(N-1)$ equations can be obtained from Equation 3.12. The Dirichlet boundary conditions are added as well to solve Equation 3.13, which can be seen in

Equation 3.14:

$$\begin{cases} \phi_0^m = H \\ \phi_N^m = 0 \end{cases}, m = 1, 2, ..., M . \tag{3.14}$$

When $t = 0$, the water head at the upstream side is H, while water heads at all other nodes are zero, which can be seen in Equation 3.15:

$$\begin{cases} \phi_0^0 = H \\ \phi_j^0 = 0 \end{cases}, j = 1, 2, ..., N . \tag{3.15}$$

Thus $(N+1)$ equations are obtained and $(N+1)$ unknowns, i.e. $(N+1)$ ϕ_j^m can be solved.

The discharge rate q_j^m at the jth node and mth time point can be calculated by Equation 3.16:

$$q_j^m = k \frac{\phi_{j+1}^m - \phi_{j-1}^m}{2\Delta y} A_j, \tag{3.16}$$

where k is the coefficient of conductivity.

Since there might be more than one penetration flow path, the total discharge rate is calculated by summing up all the discharge rates at each flow passage way separately, which is also mentioned in Pan et al. (2017, 2019a).

When there are no windows in the cutoff wall, the discharge rate is significantly lower than that when there is penetration (Pan et al., 2021), and the water-proofness shall be represented by the minimum thickness (Croce and Modoni, 2007; Pan et al., 2019b).

3.2 FEM for 1D linear transient advection-diffusion process

Equation 3.8 can be applied in contaminant diffusion problems as well, although in real foul water leakage problems, advection and diffusion need to be considered together. The advection process is the bulk movement of the groundwater which carries the contaminants with the groundwater as well, and the diffusion process describes the spread of contanminants in the groundwater (Pan et al., 2021).

In the contaminant transportation process, the coefficient of diffusivity D is defined as D_c, of which the unit is m^2/s.

Since the process is 1D, the location coordinate along the advection-diffusion path is denoted as x.

Modifying and adding an advection term to Equation 3.8 yields

$$A\frac{\partial u}{\partial t} + \frac{\partial (Avu)}{\partial x} = \frac{\partial}{\partial x}\left(DA\frac{\partial u}{\partial x}\right), \tag{3.17}$$

where $u(x,t)$ is the contaminant concentration, of which the unit is mg/m^3, and $v(x,t)$ is the cross-sectionally average seepage velocity along the advection-diffusion path, i.e. the velocity of the flow passing through the voids in the soil mass.

To simplify Equation 3.17, let A, v and D be constants, and Equation 3.17 becomes

$$\frac{\partial u}{\partial t} + v\frac{\partial u}{\partial x} = D\frac{\partial^2 u}{\partial x^2}. \tag{3.18}$$

When v in Equation 3.18 is 0, no advection happens, and it becomes the governing equation for the pure diffusion process.

Since Equation 3.17 and 3.18 can be applied in heat transfer process as well, a FEM algorithm by Schirén (2018) is used to solve Equation 3.18 numerically, and the relevant heat related parameters are replaced by the concentration related parameters.

The pollutant flux, which is the amount of pollutant transported through a unit cross-sectional area of soil per unit time, consists of the advection and diffusion parts. The pollutant flux due to advection is defined as the product of the porosity of soil n, pollutant concentration u and the seepage velocity v:

$$J_a = nuv. \tag{3.19}$$

According to Fick's first law, the pollutant flux due to diffusion in soil is

$$J_s = -nD\frac{\partial u}{\partial x}, \tag{3.20}$$

when the soil is saturated.

The total pollutant flux J is then the sum of J_a and J_s

$$J = n\left(uv - D\frac{\partial u}{\partial x}\right). \tag{3.21}$$

When u at the jth location node and the mth time point is known as u_j^m, the pollutant flux J at the jth location node and the mth time point shall be calculated as

$$J_j^m = n\left(vu_j^m - D\frac{u_{j+1}^m - u_{j-1}^m}{2\Delta x}\right). \tag{3.22}$$

where $\Delta x = \frac{T_{wall}}{N}$, and N is the number of segments.

By letting the seepage velocity be 0, the pollutant flux in the pure diffusive situation can be obtained in an analogical way.

3.3 1D steady seepage and transient pollutant advection-diffusion coupled process

The seepage process and pollutant advection-diffusion process are coupled by the seepage velocity, and the illustration for the coupled process is shown in Figure 3.7.

To describe the process, a coupled equation governing equation shall be derived and an analytical or numerical method to solve the equation is necessary.
For the 1D linear governing equation with inhomogeneous Dirichlet boundary conditions, the analytical results are given and the contaminant flux is normalized, upon which the definition and judge criterion of breakthrough time are obtained.

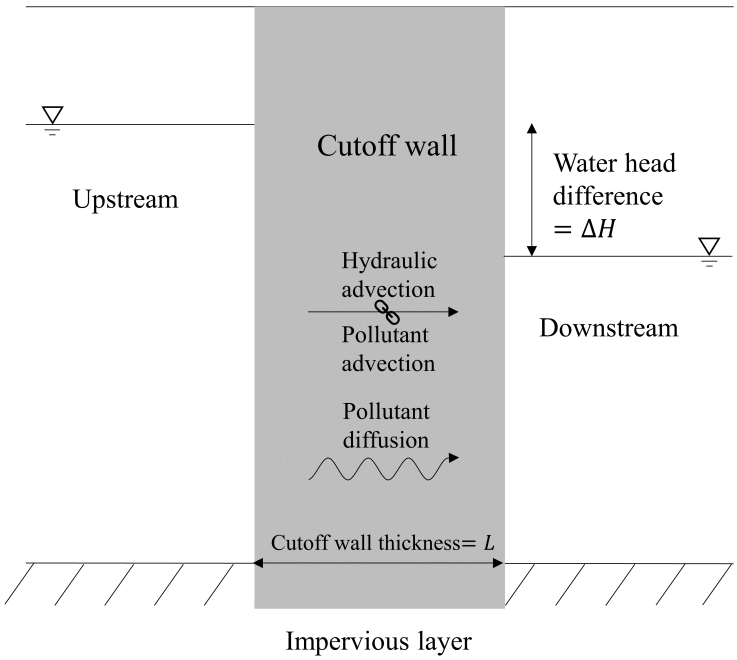

Figure 3.7: Illustration for the seepage and pollutant advection-diffusion coupled process

For the nonlinear scenario, the 1D transient contaminant advection-diffusion equation which is coupled with the inhomogeneous Dirichlet boundaried steady seepage process is deduced, and the FDM algorithm as the numerical solution and the ADM algorithm as the semi-analytical solution to the governing equation are given, although the ADM method is only feasible for few types of 1D nonlinear channels.

3.3.1 1D linear pollutant advection-diffusion problem

When the cross-sectional area along the advection-diffusion is a constant, it shall be removed from Equation 3.17, and it is possible to solve the resultant equation analytically with a constant seepage velocity v. The properties of the porous medium are regarded as uniform to faciliate the deduction, which means the hydraulic conductivity k, porosity n, and coefficient of diffusivity for seepage and contaminant diffusion D_w and D_c respectively are all constants.

3.3.1.1 Coupled equations and solution

The 1D coupled process, which is with the inhomogeneous Dirichlet boundary conditions, is described by the following coupled equation system:

$$\begin{cases} \dfrac{\partial \phi}{\partial t_1} = D_w \dfrac{\partial^2 \phi}{\partial x^2} \\ \dfrac{\partial u}{\partial t_2} + \dfrac{\partial (vu)}{\partial x} = D_c \dfrac{\partial^2 u}{\partial x^2} \end{cases} \quad (0 \leqslant x \leqslant L, t_2 \geqslant t_1 \geqslant 0), \tag{3.23}$$

where $\phi(x, t_1)$ is the water head, $u(x, t_2)$ is the pollutant concentration, t_1 is the time coordinate in the seepage process, t_2 is the time coordinate in the pollutant advection-diffusion process, $t_2 = t_1 + \Delta t$, where Δt is the time difference between the starting times of the processes, L is the length of the advection-diffusion path, which is equivalent to the nominal thickness of the cutoff wall T_{wall}, $v(x, t_1) = \frac{k}{n}\frac{\partial \phi}{\partial x}$ is the seepage velocity, $D_w = \frac{k}{\gamma_w m_v}$ is the constant coefficient of diffusivity for seepage process, and D_c is the constant coefficient of diffusivity for pollutant diffusion process.

The boundary conditions for the groundwater seepage and pollutant advection-diffusion process are shown in Equation 3.24 and 3.25 respectively:

$$\begin{cases} \phi(0, t_1) = H_u \\ \phi(L, t_1) = H_d \end{cases} \quad (t_1 > 0), \tag{3.24}$$

$$\begin{cases} u(0, t_2) = C_u \\ u(L, t_2) = C_d \end{cases} \quad (t_2 > 0), \tag{3.25}$$

where H_u and H_d are the constant upstream and downstream water head respectively, and C_u and C_d are the constant upstream and downstream pollutant concentration respectively ($H_u > H_d \geqslant 0$, $C_u > C_d \geqslant 0$).

The coupled process described by Equation 3.23 with its boundary conditions can be intuitively seen in Figure 3.8.

Since the boundary conditions are constant, the steady states exist for the two processes. In re-

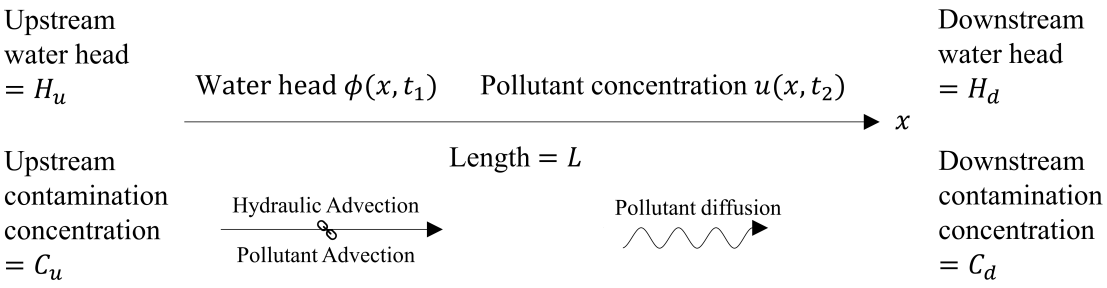

Figure 3.8: Illustration for the coupled 1D advection-diffusion process

ality, the contaminant leakage usually happens with the steady groundwater flow, which means Δt is large enough for the seepage process to be steady. Denote the steady water head as $\phi_s(x)$ and let t_1 in the seepage equation to be sufficiently large, i.e. $\frac{\partial \phi}{\partial t_1} \equiv 0$, the seepage equation in Equation 3.23 becomes

$$\frac{d^2\phi_s}{dx^2} = 0 \quad (0 \leqslant x \leqslant L). \tag{3.26}$$

Solving the ODE gives $\phi_s(x) = H_u - i_s x$, where $i_s = \frac{\Delta H}{L}$ is the steady hydraulic gradient and $\Delta H = H_u - H_d$ is the difference between the upstream and downstream water heads. Thus the steady seepage velocity v_s is

$$v_s = -\frac{k}{n}\frac{d\phi_s}{dx} = \frac{k\Delta H}{nL}. \tag{3.27}$$

Therefore it is reasonable to transform the coupled equation system into

$$\frac{\partial u}{\partial t} + v_s\frac{\partial u}{\partial x} = D_c\frac{\partial^2 u}{\partial x^2} \quad (0 \leqslant x \leqslant L, t \geqslant 0). \tag{3.28}$$

The initial condition is

$$u(x, 0) = C_d \quad (0 \leqslant x \leqslant L). \tag{3.29}$$

Then the illustration for Equation 3.28 is shown in Figure 3.9.

When $\frac{\partial u}{\partial t} \equiv 0$, i.e. the pollutant advection-diffusion process is in steady state, Equation 3.28 becomes

$$v_s\frac{du_s}{dx} = D_c\frac{d^2u_s}{dx^2} \quad (0 \leqslant x \leqslant L), \tag{3.30}$$

where $u_s(x)$ is the steady pollutant concentration at location x.

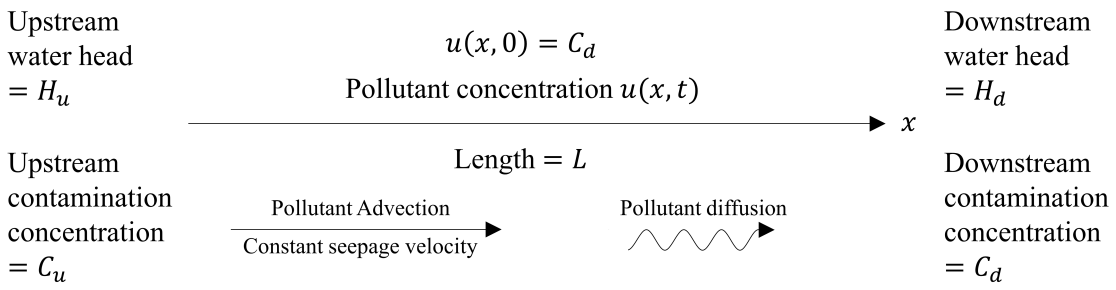

Figure 3.9: Illustration for the 1D pollutant advection-diffusion process with constant seepage velocity and initial condition

The solution to Equation 3.30 is

$$u_s(x) = C_u + \frac{\Delta C}{e^{\mathrm{Pe}} - 1}\left(1 - e^{\frac{\mathrm{Pe}}{L}x}\right), \tag{3.31}$$

where $\Delta C = C_u - C_d > 0$ and $\mathrm{Pe} = \frac{v_s L}{D_c} = \frac{k\Delta H}{nD_c}$ is the constant Péclet number which measures the importance of the advection process over the diffusion process in the transportation of pollutant mass.

To transform the inhomogeneous boundary conditions into homogeneous boundary conditions, a technique by Brown and Churchill (1993) is used. Denote $u_h(x,t) = u(x,t) - u_s(x)$, which still satisfies the Burgers equation, and boundary conditions become homogeneous:

$$\begin{cases} u_h(0,t) = 0 \\ u_h(L,t) = 0 \end{cases} \quad (t > 0)\,. \tag{3.32}$$

The new initial condition is

$$u_h(x,0) = C_d - u_s(x) = \frac{\Delta C}{e^{\mathrm{Pe}} - 1}\left(e^{\frac{\mathrm{Pe}}{L}x} - e^{\mathrm{Pe}}\right). \tag{3.33}$$

According to Guerrero et al. (2009), $u_h(x,t)$ can be tranformed as

$$u_h(x,t) = w(x,t)e^{\alpha x + \beta t}, \tag{3.34}$$

where $\alpha = \frac{v_s}{2D_c} = \frac{\mathrm{Pe}}{2L}$ and $\beta = -\frac{v_s^2}{4D_c} = -\frac{D_c}{4}\left(\frac{\mathrm{Pe}}{L}\right)^2$.

Then Equation 3.28 is reduced to

$$\frac{\partial w}{\partial t} = D_c \frac{\partial^2 w}{\partial x^2} \quad (0 \leqslant x \leqslant L, t \geqslant 0). \tag{3.35}$$

The boundary conditions therefore become

$$\begin{cases} w(0,t) = 0 \\ w(L,t) = 0 \end{cases} \quad (t > 0)\,. \tag{3.36}$$

and the initial condition for Equation 3.35 is

$$w(x,0) = e^{-\alpha x} u_h(x,0) = \frac{\Delta C}{e^{\mathrm{Pe}} - 1}\left[e^{\frac{\mathrm{Pe}}{2L}x} - e^{\frac{\mathrm{Pe}}{L}\left(L-\frac{x}{2}\right)}\right]. \tag{3.37}$$

By the method of separation of variables and set $w(x,t) = X(x)T(t)$, the solution to Equation 3.35 is (Brown and Churchill, 1993; Mojtabi and Deville, 2015)

$$w(x,t) = \sum_{j=0}^{\infty}\left[B_j \sin\left(\frac{j\pi x}{L}\right) + C_j \cos\left(\frac{j\pi x}{L}\right)\right] e^{-\left(\frac{j\pi}{L}\right)^2 D_c t}. \tag{3.38}$$

Substituting the boundary conditions 3.36 into Equation 3.38 gives $C_j = 0$, and Equation 3.38 becomes

$$w(x,t) = \sum_{j=1}^{\infty} B_j \sin\left(\frac{j\pi x}{L}\right) e^{-\left(\frac{j\pi}{L}\right)^2 D_c t}. \tag{3.39}$$

Using the initial condition 3.37 gives

$$\sum_{j=1}^{\infty} B_j \sin\left(\frac{j\pi x}{L}\right) = \frac{\Delta C}{e^{\mathrm{Pe}} - 1}\left[e^{\frac{\mathrm{Pe}}{2L}x} - e^{\frac{\mathrm{Pe}}{L}\left(L-\frac{x}{2}\right)}\right]. \tag{3.40}$$

Multiplying $\sin\left(\frac{k\pi x}{L}\right)$ at both sides of Equation 3.40, where $k \in \mathbb{Z}^+$, it can be obtained that

$$\sum_{j=1}^{\infty} B_j \sin\left(\frac{j\pi x}{L}\right)\sin\left(\frac{k\pi x}{L}\right) = \frac{\Delta C}{e^{\mathrm{Pe}} - 1}\sin\left(\frac{k\pi x}{L}\right)\left[e^{\frac{\mathrm{Pe}}{2L}x} - e^{\frac{\mathrm{Pe}}{L}\left(L-\frac{x}{2}\right)}\right]. \tag{3.41}$$

The definite integral of both sides of Equation 3.41 from 0 to L yields

$$\sum_{j=1}^{\infty} B_j \int_0^L \sin\left(\frac{j\pi x}{L}\right)\sin\left(\frac{k\pi x}{L}\right) dx = \frac{\Delta C}{e^{\mathrm{Pe}} - 1}\int_0^L \sin\left(\frac{k\pi x}{L}\right)\left[e^{\frac{\mathrm{Pe}}{2L}x} - e^{\frac{\mathrm{Pe}}{L}\left(L-\frac{x}{2}\right)}\right] dx. \tag{3.42}$$

Applying the product to sum formulas of trigonometry gives

$$\int_0^L \sin\left(\frac{j\pi x}{L}\right)\sin\left(\frac{k\pi x}{L}\right)dx = -\frac{1}{2}\int_0^L \left\{\cos\left[\frac{(j+k)\pi x}{L}\right] - \cos\left[\frac{(j-k)\pi x}{L}\right]\right\}dx. \tag{3.43}$$

When $j \neq k$, the right side of Equation 3.43 becomes

$$\int_0^L \left\{\cos\left[\frac{(j+k)\pi x}{L}\right] - \cos\left[\frac{(j-k)\pi x}{L}\right]\right\}dx = 0. \tag{3.44}$$

When $j = k$, it becomes

$$\int_0^L \left\{\cos\left[\frac{(j+k)\pi x}{L}\right] - \cos\left[\frac{(j-k)\pi x}{L}\right]\right\}dx = \int_0^L \left[\cos\left(\frac{2k\pi x}{L}\right) - 1\right]dx = -L. \tag{3.45}$$

Then the left side of Equation 3.43 is

$$\int_0^L \sin\left(\frac{j\pi x}{L}\right)\sin\left(\frac{k\pi x}{L}\right)dx = \begin{cases} 0, & j \neq k \\ \dfrac{L}{2}, & j = k \end{cases}, \tag{3.46}$$

and Equation 3.42 becomes

$$B_k \int_0^L \sin^2\left(\frac{k\pi x}{L}\right)dx = \frac{\Delta C}{e^{\mathrm{Pe}} - 1}\int_0^L \sin\left(\frac{k\pi x}{L}\right)\left[e^{\frac{\mathrm{Pe}}{2L}x} - e^{\frac{\mathrm{Pe}}{L}\left(L-\frac{x}{2}\right)}\right]dx. \tag{3.47}$$

The result of the integral part at the right side of Equation 3.47 is

$$\int_0^L \sin\left(\frac{k\pi x}{L}\right)\left[e^{\frac{\mathrm{Pe}}{2L}x} - e^{\frac{\mathrm{Pe}}{L}\left(L-\frac{x}{2}\right)}\right]dx = \frac{4k\pi L}{\mathrm{Pe}^2 + (2k\pi)^2}\left(1 - e^{\mathrm{Pe}}\right). \tag{3.48}$$

Combining Equation 3.46, 3.47 and 3.48 gives

$$B_k = -\frac{8k\pi\Delta C}{\mathrm{Pe}^2 + (2k\pi)^2}. \tag{3.49}$$

Therefore, $w(x,t)$, $u_h(x,t)$ and $u(x,t)$ can be obtained by backstepping, which can be seen in Equation 3.50, 3.51 and 3.52 respectively, and Equation 3.52 agrees with the result of the first test case in Guerrero et al. (2009).

$$w(x,t) = -8\pi\Delta C\sum_{j=1}^{\infty}\frac{j}{\mathrm{Pe}^2 + (2j\pi)^2}\sin\left(\frac{j\pi x}{L}\right)e^{-\left(\frac{j\pi}{L}\right)^2 D_c t} \tag{3.50}$$

$$u_h(x,t) = -8\pi\Delta C \sum_{j=1}^{\infty} \frac{j}{\mathrm{Pe}^2 + (2j\pi)^2} \sin\left(\frac{j\pi x}{L}\right) e^{\frac{\mathrm{Pe}}{2L}x - \frac{D_c}{(2L)^2}[\mathrm{Pe}^2 + (2n\pi)^2]t} \tag{3.51}$$

$$u(x,t) = C_u + \frac{\Delta C}{1-e^{\mathrm{Pe}}}\left(e^{\frac{\mathrm{Pe}}{L}x} - 1\right) - 8\pi\Delta C \sum_{j=1}^{\infty} \frac{j}{\mathrm{Pe}^2 + (2j\pi)^2} \sin\left(\frac{j\pi x}{L}\right) e^{\frac{\mathrm{Pe}}{2L}x - \frac{D_c}{(2L)^2}\left[\mathrm{Pe}^2 + (2j\pi)^2\right]t} \tag{3.52}$$

When v_s approaches 0, Pe goes to 0, and the Burgers equation is reduced to the equation of the Fick's second law, of which the solution 3.53 can be obtained by letting Pe in Equation 3.52 approach 0:

$$u(x,t) = C_u - \frac{\Delta C}{L}x - \frac{2\Delta C}{\pi} \sum_{j=1}^{\infty} \frac{1}{j} e^{-\left(\frac{j\pi}{L}\right)^2 D_c t} \sin\left(\frac{j\pi x}{L}\right). \tag{3.53}$$

Similarly, when the initial condition for the seepage equation in Equation 3.23 is

$$\phi(x,0) = H_d \quad (0 \leqslant x \leqslant L), \tag{3.54}$$

the seepage equation can be solved as

$$\phi(x,t) = H_u - i_s x - \frac{2\Delta H}{\pi} \sum_{j=1}^{\infty} \frac{1}{j} e^{-\left(\frac{j\pi}{L}\right)^2 D_w t_s} \sin\left(\frac{j\pi x}{L}\right), \tag{3.55}$$

where t_s is the time coordinate for the seepage process.

The hydraulic gradient is obtained through the derivation of Equation 3.55:

$$i(x,t) = -i_s\left[1 + 2\sum_{j=1}^{\infty} e^{-\left(\frac{j\pi}{L}\right)^2 D_w t_s} \cos\left(\frac{j\pi x}{L}\right)\right] = -i_s \vartheta_3(z,q), \tag{3.56}$$

where $\vartheta_3(z,q) = 1 + 2\sum_{j=1}^{\infty} q^{j^2}\cos(2jz)$ is a Jacobi theta function, with $z = \frac{\pi}{2L}x$ and $q = e^{-\left(\frac{\pi}{L}\right)^2 D_w t_s}$ (Jacobi, 1829; Whittaker and Watson, 1962).

The value of seepage velocity is

$$v = v_s\left[1 + 2\sum_{j=1}^{\infty} e^{-\left(\frac{j\pi}{L}\right)^2 D_w t_s} \cos\left(\frac{j\pi x}{L}\right)\right] = v_{ss}\vartheta_3\left[\frac{\pi}{2L}x, e^{-\left(\frac{\pi}{L}\right)^2 D_w t_s}\right] \tag{3.57}$$

Let t_s approach positive infinity and it is verified that $v = v_s$.

3.3.1.2 Derivation of normalized polltant flux

It is necessary to normalize the time and pollutant flux to simplify the formulas and faciliate the plotting of the pollutant flux diagrams.

3.3.1.2.1 Theoretical normalized pollutant flux

According to Equation 3.21, the total pollutan flux for the coupled process described by Equation 3.28 shall be obtained as

$$J = n\left(uv_s - D_c\frac{\partial u}{\partial x}\right). \tag{3.58}$$

The steady concentration gradient can be obtained from the deriviation of Equation 3.31:

$$\frac{\partial u_s}{\partial x} = \frac{\Delta C}{L}\frac{\mathrm{Pe}}{1-e^{\mathrm{Pe}}}e^{\frac{\mathrm{Pe}}{L}x}, \tag{3.59}$$

therefore the steady contamination gradient at the upstream inlet is

$$\frac{\partial u_s}{\partial x} = \frac{\Delta C}{L}\frac{\mathrm{Pe}}{1-e^{\mathrm{Pe}}}, \tag{3.60}$$

and the contamination gradient at the downstream outlet in steady state is

$$\frac{\partial u_s}{\partial x} = \frac{\Delta C}{L}\frac{\mathrm{Pe}}{1-e^{\mathrm{Pe}}}e^{\mathrm{Pe}}. \tag{3.61}$$

The concentration at the downstream outlet is assumed to be 0, hence the steady total pollutant flux at the upstream inlet J_{su} is

$$J_{su} = n\left(C_u v_s + D_c\frac{C_u}{L}\frac{\mathrm{Pe}}{e^{\mathrm{Pe}}-1}\right) = nD_c\frac{C_u}{L}\left(\mathrm{Pe}+\frac{\mathrm{Pe}}{e^{\mathrm{Pe}}-1}\right) = \lambda J_{spd}, \tag{3.62}$$

and the downstream flux J_{sd} is

$$J_{sd} = nD_c\frac{C_u}{L}\frac{\mathrm{Pe}}{e^{\mathrm{Pe}}-1}e^{\mathrm{Pe}} = \lambda J_{spd}, \tag{3.63}$$

where $J_{spd} = nD_c\frac{\Delta C}{L} = nD_c\frac{C_u}{L}$ is the steady pollutant flux when there is only diffusion, i.e. the

pure diffusion flux, and the ratio of J_{sd} to J_{spd} is defined as

$$\lambda = \frac{J_{sd}}{J_{spd}} = \frac{\mathrm{Pe}}{e^{\mathrm{Pe}} - 1} e^{\mathrm{Pe}}. \tag{3.64}$$

Apparently the steady pollutant fluxes at the upstream inlet and downstream outlet are equal. Since the cross-sectional area is uniform, in steady state the conservation law of pollutant mass is verified.

It can be seen from Figure 3.10 that when $\mathrm{Pe} \leqslant 0.1$, λ is approximately 1, and when $\mathrm{Pe} > 5$, λ is close to Pe. Therefore the approximation of J_{sd} can be obtained in Equation 3.65:

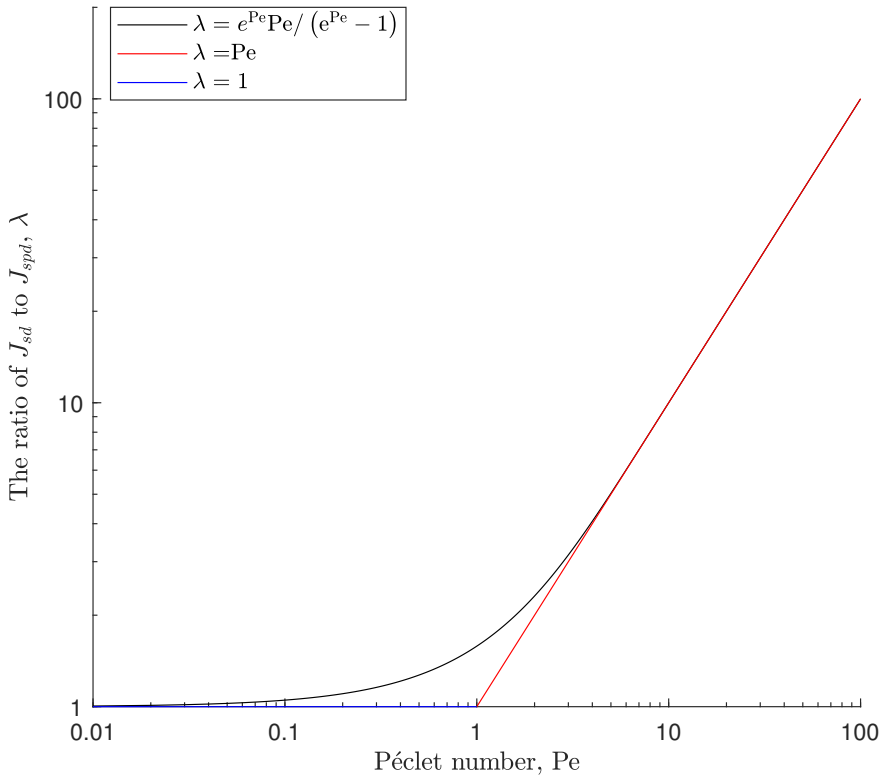

Figure 3.10: Plot of the ratio of downstream flux J_{sd} to the pure diffusion downstream flux J_{spd} versus the Péclet number Pe

$$\begin{cases} J_{sd} = J_{spd} & \text{when } \mathrm{Pe} \leqslant 0.1 \\ J_{sd} = \lambda J_{spd} & \text{when } 0.1 < \mathrm{Pe} < 5 \\ J_{sd} = \mathrm{Pe} J_{spd} & \text{when } \mathrm{Pe} \geqslant 5 \end{cases}. \tag{3.65}$$

The derivation of Equation 3.52 gives the transient concentration gradient, which is in Equation 3.66:

$$\begin{aligned}\frac{\partial u}{\partial x} =& -\frac{C_u}{L}\left\{\lambda e^{\mathrm{Pe}\left(\frac{x}{L}-1\right)}\right.\\ &\left.+8\pi\sum_{j=1}^{\infty}\frac{j}{\mathrm{Pe}^2+\left(2j\pi\right)^2}\left[j\pi\cos\left(\frac{j\pi x}{L}\right)+\frac{\mathrm{Pe}}{2}\sin\left(\frac{j\pi x}{L}\right)\right]e^{\frac{\mathrm{Pe}}{2L}x-\frac{D_c}{(2L)^2}\left[\mathrm{Pe}^2+(2j\pi)^2\right]t}\right\},\end{aligned} \tag{3.66}$$

where the minus value of $\frac{\partial u}{\partial x}$ means the transportation of pollutant is towards the positive x-direction.

The transient pollutant flux is

$$\begin{aligned}J =& nC_u v_s\left\{1+\frac{1}{1-e^{\mathrm{Pe}}}\left(e^{\frac{\mathrm{Pe}}{L}x}-1\right)\right.\\ &\left.-8\pi\sum_{j=1}^{\infty}\frac{j}{\mathrm{Pe}^2+(2j\pi)^2}\sin\left(\frac{j\pi x}{L}\right)e^{\frac{\mathrm{Pe}}{2L}x-\frac{D_c}{(2L)^2}\left[\mathrm{Pe}^2+(2j\pi)^2\right]t}\right\}+nD_c\frac{C_u}{L}\left\{\lambda e^{\mathrm{Pe}\left(\frac{x}{L}-1\right)}+\right.\\ &\left.8\pi\sum_{j=1}^{\infty}\frac{j}{\mathrm{Pe}^2+\left(2j\pi\right)^2}\left[j\pi\cos\left(\frac{j\pi x}{L}\right)+\frac{\mathrm{Pe}}{2}\sin\left(\frac{j\pi x}{L}\right)\right]e^{\frac{\mathrm{Pe}}{2L}x-\frac{D_c}{(2L)^2}\left[\mathrm{Pe}^2+(2j\pi)^2\right]t}\right\}\\ =&\mathrm{Pe}J_{spd}\left\{1+\frac{1}{1-e^{\mathrm{Pe}}}\left(e^{\frac{\mathrm{Pe}}{L}x}-1\right)\right.\\ &\left.-8\pi\sum_{j=1}^{\infty}\frac{j}{\mathrm{Pe}^2+(2j\pi)^2}\sin\left(\frac{j\pi x}{L}\right)e^{\frac{\mathrm{Pe}}{2L}x-\frac{D_c}{(2L)^2}\left[\mathrm{Pe}^2+(2j\pi)^2\right]t}\right\}+J_{spd}\left\{\lambda e^{\mathrm{Pe}\left(\frac{x}{L}-1\right)}\right.\\ &\left.+8\pi\sum_{j=1}^{\infty}\frac{j}{\mathrm{Pe}^2+\left(2j\pi\right)^2}\left[j\pi\cos\left(\frac{j\pi x}{L}\right)+\frac{\mathrm{Pe}}{2}\sin\left(\frac{j\pi x}{L}\right)\right]e^{\frac{\lambda}{2L}x-\frac{D_c}{(2L)^2}\left[\mathrm{Pe}^2+(2j\pi)^2\right]t}\right\}\\ =&J_{spd}\left\{\lambda+8\pi\sum_{j=1}^{\infty}\frac{j}{\mathrm{Pe}^2+\left(2j\pi\right)^2}\left[j\pi\cos\left(\frac{j\pi x}{L}\right)-\frac{\mathrm{Pe}}{2}\sin\left(\frac{j\pi x}{L}\right)\right]e^{\frac{\mathrm{Pe}}{2L}x-\frac{D_c}{(2L)^2}\left[\mathrm{Pe}^2+(2j\pi)^2\right]t}\right\}\\ =&J_{sd}\left\{1+\frac{8\pi}{\lambda}\sum_{j=1}^{\infty}\frac{j}{\mathrm{Pe}^2+\left(2j\pi\right)^2}\left[j\pi\cos\left(\frac{j\pi x}{L}\right)-\frac{\mathrm{Pe}}{2}\sin\left(\frac{j\pi x}{L}\right)\right]e^{\frac{\mathrm{Pe}}{2L}x-\frac{D_c}{(2L)^2}\left[\mathrm{Pe}^2+(2j\pi)^2\right]t}\right\}.\end{aligned} \tag{3.67}$$

To normalize time t, define the characteristic time for normalization as $T=\frac{L^2}{D_c}$, and the normalized time is $\hat{t}=\frac{t}{T}$. Therefore the Péclet number is defined in another way as $\mathrm{Pe}=\frac{v_s T}{L}$, which indicates Pe is the ratio of the distance the advection wave has traveled at a velocity v_s within the characteristic time T to the length L. The pollutant flux is normalized as $\hat{J}=\frac{J}{J_{sd}}$, which is shown in Equation 3.68:

$$\hat{J}=1+\frac{8\pi}{\lambda}\sum_{j=1}^{\infty}\frac{j}{\mathrm{Pe}^2+\left(2j\pi\right)^2}\left[j\pi\cos\left(\frac{j\pi x}{L}\right)-\frac{\mathrm{Pe}}{2}\sin\left(\frac{j\pi x}{L}\right)\right]e^{\frac{\mathrm{Pe}}{2L}x-\left[\left(\frac{\mathrm{Pe}}{2}\right)^2+(j\pi)^2\right]\hat{t}}. \tag{3.68}$$

Therefore, the normalized transient pollutant fluxes at the upstream inlet and the downstream outlet can be derived as Equation 3.69 and 3.70 respectively:

$$\hat{J}_u = 1 + \frac{8\pi^2}{\lambda} \sum_{j=1}^{\infty} \frac{j^2}{\mathrm{Pe}^2 + (2j\pi)^2} e^{-\left[\left(\frac{\mathrm{Pe}}{2}\right)^2 + (j\pi)^2\right]\hat{t}} \tag{3.69}$$

$$\hat{J}_d = 1 + \frac{8\pi^2}{\lambda} \sum_{j=1}^{\infty} \frac{(-1)^j j^2}{\mathrm{Pe}^2 + (2j\pi)^2} e^{\frac{\mathrm{Pe}}{2} - \left[\left(\frac{\mathrm{Pe}}{2}\right)^2 + (j\pi)^2\right]\hat{t}}. \tag{3.70}$$

Let Pe in Equation 3.68 be 0, and the normalized flux in pure diffusion scenario is

$$\hat{J}_{pd} = 1 + 2\sum_{j=1}^{\infty} e^{-(j\pi)^2\hat{t}} \cos\left(\frac{j\pi x}{L}\right) = \vartheta_3\left(\frac{\pi}{2L}x, e^{-\pi^2\hat{t}}\right). \tag{3.71}$$

The normalized transient upstream and downstream pollutant fluxes in pure diffusion scenario are expressed in Equation 3.72 and 3.73 respectively:

$$\hat{J}_{pdu} = 1 + 2\sum_{j=1}^{\infty} e^{-(j\pi)^2\hat{t}} = \vartheta_3\left(0, e^{-\pi^2\hat{t}}\right) \tag{3.72}$$

$$\hat{J}_{pdd} = 1 + 2\sum_{j=1}^{\infty} (-1)^j e^{-(j\pi)^2\hat{t}} = \vartheta_3\left(\frac{\pi}{2}, e^{-\pi^2\hat{t}}\right). \tag{3.73}$$

3.3.1.2.2 Numerical normalized pollutant flux

The normalized pollutant flux is

$$\hat{J}_j^m = \frac{J_j^m}{J_{sd}} = \frac{1}{C_u\lambda}\left[\mathrm{Pe}u_j^m - \frac{N}{2}\left(u_{j+1}^m - u_{j-1}^m\right)\right]. \tag{3.74}$$

Thus the normalized upstream pollutant flux is

$$\hat{J}_2^m = \frac{1}{C_u\lambda}\left[\mathrm{Pe}u_2^m - \frac{N}{2}\left(u_3^m - u_1^m\right)\right], \tag{3.75}$$

and the normalized downstream pollutant flux is

$$\hat{J}_{N-1}^m = \frac{1}{C_u\lambda}\left[\mathrm{Pe}u_{N-1}^m - \frac{N}{2}\left(u_N^m - u_{N-2}^m\right)\right]. \tag{3.76}$$

3.3.1.3 Breakthrough time

The breakthrough time t_b is defined as the time required for the pollutant concentration at the downstream outlet to reach a regulated limit value (Chen et al., 2015; Ding et al., 2020). In some scenarios, when there are huge amounts of water at the downstream outlet to dilute the leakachate, such as lake or sea, the pollutant concentration at the downstream outlet is 0, which is also the boundary condition for Equation 3.23. Therefore the definion by Chen et al. (2015) needs to be modified.

The pollutant mass discharge rate MDR is defined as the amount of pollutant mass passing through a cross-section per unit time, and is the product of the pollutant flux and the cross-sectional area. It is necessary to regulate the limit value for the pollutant discharge rate at the downstream outlet, which is denoted as $\mathrm{MDR}_{\mathrm{lim}}$ here, and the breakthrough time is defined as the time required for the pollutant discharge rate at the downstream outlet to reach $\mathrm{MDR}_{\mathrm{lim}}$. Denote the cross-sectional area as A and the normalized limit for pollutant mass discharge rate is $\widehat{\mathrm{MDR}}_{\mathrm{lim}} = \frac{\mathrm{MDR}_{\mathrm{lim}}}{AJ_{sd}} = \frac{\mathrm{MDR}_{\mathrm{lim}}L}{nD_cC_u\lambda A}$. When $\widehat{\mathrm{MDR}}_{\mathrm{lim}} > 1$, which means the steady pollutant mass discharge rate at the downstream outlet $\mathrm{MDR}_{sd} = AJ_{sd}$ is larger than $\mathrm{MDR}_{\mathrm{lim}}$, penetration happensm, and the judge criterion is defined as

$$\hat{J}_{bd} = \widehat{\mathrm{MDR}}_{\mathrm{lim}}, \tag{3.77}$$

where $\hat{J}_{bd}$ is the downstream flux at the breakthrough time t_b, and Equation 3.77 indicates that the breakthrough time t_b is the critical moment when the downstream pollutant flux reaches a cartain proportion of the steady pollutant flux, which is $\widehat{\mathrm{MDR}}_{\mathrm{lim}}$.

Subsititution of Equation 3.70 gives

$$1 - \widehat{\mathrm{MDR}}_{\mathrm{lim}} + \frac{8\pi^2}{\lambda}\sum_{j=1}^{\infty}\frac{(-1)^j j^2}{\mathrm{Pe}^2 + (2j\pi)^2} e^{\frac{\mathrm{Pe}}{2} - \left[\left(\frac{\mathrm{Pe}}{2}\right)^2 + (j\pi)^2\right]\hat{t}_b} = 0, \tag{3.78}$$

where $\hat{t}_b$ is the normalized breakthrough time.

Since $\hat{J}_d$ is monotonous regarding $\hat{t}$, when Pe, $\widehat{\mathrm{MDR}}_{\mathrm{lim}}$ are known, $\hat{t}_b$ can be calculated by checking the sign changing location in the numerical array of the left hand side of Equation 3.78 as a

function regarding the normalized time $\hat{t}$.

However, from Table 3.2 it can be seen that the value of Pe can vary from 0 to 1×10^6 when the water head difference ΔH is regarded to range from 0 meter to 20 meters, and when Pe is too large or too small, it is difficult to calculate the lefthand side of Equation 3.78 numerically. Thus approximations is necessary to obtain $\hat{t}_b$ in these two situations.

Table 3.2: Typical parameters for Qizishan landfill in Suzhou (Zhan et al., 2013)

Soil layers	**Hydraulic conductivity k unit: cm/s**	**Coefficient of diffusivity D_c unit : m^2/s**	**Distribution coefficient K unit : mL/g**	**Dispersivity α unit: m**	**Porosity n unit : %**	**Dry density ρ_d unit : g/cm^3**
Plain fill	8×10^{-4}	6×10^{-10}	1	0.1	44	1.5
Silty clay	1.4×10^{-4}	3.5×10^{-10}	3	0.1	41	1.6
Highly-moderately weathered bedrock	2.8×10^{-5}	2.5×10^{-10}	3	0.1	20	2.0
Slightly-none weathered bedrock	1×10^{-8}	1.5×10^{-10}	5	0.1	20	2.5
Low quality waterproof curtain	1×10^{-6}	2.5×10^{-10}	5	0.1	35	2.2
Standard quality water proof curtain	1×10^{-7}	2×10^{-10}	5	0.1	30	2.3
High quality water proof curtain	1×10^{-8}	1.5×10^{-10}	5	0.1	30	2.4
Anti pollution dam	1×10^{-8}	2.5×10^{-10}	5	0.1	30	2.4

3.3.1.3.1 When Pe is large enough

The diffusion process is negligible in this situation and the governing equation becomes

$$\frac{\partial u}{\partial t} + v_s \frac{\partial u}{\partial x} = 0 \quad (0 \leqslant x \leqslant L, t \geqslant 0)\,. \tag{3.79}$$

With the inhomogeneous Dirichlet boundary conditions 3.25 and initial condition 3.29, the solution to Equation 3.79 is simply

$$\begin{cases} u(x,t) = C_u & \text{when } x - v_s t \leqslant 0 \\ u(x,t) = C_d & \text{when } x - v_s t > 0 \end{cases} \quad (0 \leqslant x \leqslant L, t \geqslant 0)\,. \tag{3.80}$$

Therefore it is obvious that the normalized breakthrough time $\hat{t}_b = \frac{L}{v_s T} = \frac{1}{\mathrm{Pe}}$ when penetration happens, and the judge criterion for penetration is shown in Equation 3.81:

$$\widehat{\mathrm{MDR}}_{\mathrm{lim}} = \frac{\mathrm{MDR}_{\mathrm{lim}}}{nC_u v_s A} = \frac{\mathrm{MDR}_{\mathrm{lim}}}{\mathrm{Pe} J_{spd} A} \leqslant 1. \tag{3.81}$$

3.3.1.3.2 When Pe is small enough

The advection process is ignored in this situation, and only the diffusion process is considered. Thus, Equation 3.73 is applied for the breakthrough time calculation, and the judge criterion is shown in Equation 3.82:

$$1 - \widehat{\mathrm{MDR}}_{\mathrm{lim}} + 1 + 2\sum_{j=1}^{\infty} e^{-(j\pi)^2 \hat{t}_b} = 0. \tag{3.82}$$

It can be seen that Equation 3.82 does not include Pe and $\widehat{\mathrm{MDR}}_{\mathrm{lim}}$ is the only parameter, which means when Pe is small enough, it is considered to be not concerned with the breakthrough time.

3.3.2 1D nonlinear pollutant advection-diffusion problem

When the cross-sectional area is assumed to be a variable $A(x)$, the governing equation becomes nonlinear, and a different method should be applied to find the solution.

3.3.2.1 Derivation of governing equation

Since the seepage process is generally regarded to be in steady state when coupled with the pollutant advection-diffusion process, the seepage velocity shall be defined as a variable $v_s(x)$. Therefore the nonlinear governing equation should be

$$A\frac{\partial u}{\partial t} + \frac{\partial (A v_s u)}{\partial x} = D_c \frac{\partial}{\partial x}\left(A\frac{\partial u}{\partial x}\right) \quad (0 \leqslant x \leqslant L, t \geqslant 0). \tag{3.83}$$

Since $v_s(x) = \frac{k}{n} i_s(x)$, Equation 3.83 becomes

$$A\frac{\partial u}{\partial t} + \frac{k}{n}\frac{\partial (A i_s u)}{\partial x} = D_c \frac{\partial}{\partial x}\left(A\frac{\partial u}{\partial x}\right) \quad (0 \leqslant x \leqslant L, t \geqslant 0), \tag{3.84}$$

where $i_s(x)$ is the steady hydraulic gradient.

From Equation 3.2 it can be obtained that:

$$A(x)\, i_s(x) = \frac{Q_s}{k}, \tag{3.85}$$

where Q_s is the constant steady flow rate.

Substitution of Equation 3.85 into Equation 3.84 yields

$$A\frac{\partial u}{\partial t} + \frac{Q_s}{n}\frac{\partial u}{\partial x} = D_c\frac{\partial}{\partial x}\left(A\frac{\partial u}{\partial x}\right) \quad (0 \leqslant x \leqslant L, t \geqslant 0), \tag{3.86}$$

where $Q_s = \frac{k\Delta H}{L}\tilde{A}(L)$ is obtained from Equation 3.5, of which the boundary conditions are Equation 3.24, and $\tilde{A}(L) = \frac{1}{\frac{1}{L}\int_0^L \frac{1}{A(x)}dx}$ is the harmonic average area along the advection-diffusion path.

Therefore Equation 3.86 is the governing equation for the nonlinear pollutant advection-diffusion process with inhomogeneous Dirichlet water head boundary conditions.

Expanding Equation 3.86 gives

$$\frac{\partial u}{\partial t} + r\frac{\partial u}{\partial x} = D_c\frac{\partial^2 u}{\partial x^2}, \tag{3.87}$$

where $r(x) = \frac{1}{A}\left(\frac{Q_s}{n} - D_c\frac{dA}{dx}\right)$.

Substitution of Q_s and $\tilde{A}(L)$ into $r(x)$ gives

$$r(x) = \frac{1}{A}\left(\frac{Q_s}{n} - D_c\frac{dA}{dx}\right) = \frac{1}{A}\left[\frac{k\Delta H}{nL}\tilde{A}(L) - D_c\frac{dA}{dx}\right]. \tag{3.88}$$

3.3.2.2 FDM for the nonlinear governing equation

The FDM method, which is similar to the FDM algorithm in Pan et al. (2021), is applied to discretize Equation 3.87.

The time and space are divided into M and N segments respectively, and the finite-differenced results are shown in

$$\begin{cases} \dfrac{\partial u}{\partial t} = \dfrac{u_j^{m+1} - u_j^m}{\Delta t} \\ r_j = \dfrac{D_c}{A_j L}\left[\dfrac{k\Delta H}{nD_c}\tilde{A}(L) - \dfrac{N}{2}\left(A_{j+1} - A_{j-1}\right)\right] \\ \dfrac{\partial u}{\partial x} = \dfrac{u_{j+1}^m - u_{j-1}^m}{2\Delta x} \\ \dfrac{\partial^2 u}{\partial x^2} = \dfrac{u_{j+1}^m - 2u_j^m + u_{j-1}^m}{\Delta x^2} \end{cases}, \tag{3.89}$$

where u_j^m is the pollutant concentration at the jth location node and mth time node, $\Delta x = \frac{L}{N}$, $\Delta t = \frac{T_{tot}}{M}$, $\tilde{A}(L) = \frac{1}{\frac{1}{N+1}\sum_{j=0}^{N}\frac{1}{A_j}}$ and T_{tot} is the total time for the process.

Subsititution of Equation 3.89 into Equation 3.87 yields

$$\frac{u_j^{m+1} - u_j^m}{\Delta t} + r_j\frac{u_{j+1}^m - u_{j-1}^m}{2\Delta x} = D_c\frac{u_{j+1}^m - 2u_j^m + u_{j-1}^m}{\Delta x^2}, \tag{3.90}$$

Rearrangement of Equation 3.90 gives

$$u_j^{m+1} = u_j^m + \frac{D_c\Delta t}{\Delta x^2}\left[\left(1 - \frac{r_j\Delta x}{2D_c}\right)u_{j+1}^m - 2u_j^m + \left(1 + \frac{r_j\Delta x}{2D_c}\right)u_{j-1}^m\right]. \tag{3.91}$$

When the boundary and initial conditions are known, such as the inhomogeneous Dirichlet boundary conditions in Equation 3.92 and the initial condition in Equation 3.93, u_j^m can be solved by Equation 3.91:

$$\begin{cases} u_0^m = C_u \\ u_N^m = C_d \end{cases}, m = 1, 2, ..., M, \tag{3.92}$$

$$\begin{cases} u_0^0 = C_u \\ u_j^0 = C_d \end{cases}, j = 1, 2, ..., N. \tag{3.93}$$

Since the steady seepage velocity at location x is $v_s(x) = \frac{Q_s}{nA(x)} = \frac{k\Delta H}{nLA(x)}\tilde{A}(L)$, the discretized steady seepage velocity at the jth location node is

$$(v_s)_j = \frac{k\Delta H}{nLA_j}\frac{\tilde{A}(L)}{A_j}, \tag{3.94}$$

and the discretized pollutant flux at the jth location node and mth time node is

$$J_j^m = \frac{k\Delta H}{L}\frac{\tilde{A}(L)}{A_j}u_j^m - nD_c\frac{u_{j+1}^m - u_{j-1}^m}{2\Delta x}. \tag{3.95}$$

The pollutant mass discharge rate MDR_j^m at the jth node and mth time point can be calculated by Equation 3.96:

$$\mathrm{MDR}_j^m = \frac{k\Delta H}{L}\tilde{A}(L)\,u_j^m - nD_c\frac{u_{j+1}^m - u_{j-1}^m}{2\Delta x}A_j. \tag{3.96}$$

The downstream pollutant mass discharge rate is approximated as

$$\mathrm{MDR}_{N-1}^m = \frac{k\Delta H}{L}\tilde{A}(L)\,u_{N-1}^m - nD_c\frac{u_N^m - u_{N-2}^m}{2\Delta x}A_{N-1}. \tag{3.97}$$

When multi advection-diffusion paths exist, the total pollutant mass discharge rate at the downtream outlet is the sum of all individual downstream pollutant mass discharge rates.

Since the discretized cross-sectional areas A_j for a channel in flow penetrated cutoff walls can be obtained from the simulation of randomly defective JGCOW and diaphragm walls by TDA (Pan et al., 2019a,b) or other models, the nonlinear algorithm can be coupled with the discretized cross-sectional areas A_j to assess the leakage risk for cutoff walls with stochastic construction errors in a more realistic way.

3.3.2.3 A trial on the nonlinear governing equation with ADM

The Adomian decomposition method (ADM) (Adomian, 1984, 1986a,b, 1988, 1989, 1994, 1997) is applied to give a trial on Equation 3.87.

Define $L_t u = \frac{\partial u}{\partial t}$, $L_{xx} = \frac{\partial^2 u}{\partial x^2}$ and $Nu = r\frac{\partial u}{\partial x}$.

The method by Mamaloukas (2000) is used, and rearranging Equation 3.87 gives

$$L_t u = DL_{xx}u - Nu, \tag{3.98}$$

and

$$L_{xx}u = D^{-1}(L_t u + Nu). \tag{3.99}$$

Applying the inverse operators $L_t^{-1}(.) = \int (.)\, dt$ and $L_{xx}^{-1}(.) = \int\int (.)\, dxdx$ on both sides of Equation 3.98 and 3.99 respectively gives

$$u = a_0 + L_t^{-1}\left(DL_{xx}u - Nu\right), \tag{3.100}$$

and

$$u = b_0 + D^{-1}L_{xx}^{-1}\left(L_t u + Nu\right), \tag{3.101}$$

where a_0 and b_0 are the solutions to the equations $\frac{\partial u}{\partial t} = 0$ and $\frac{\partial^2 u}{\partial x^2} = 0$ with the boundary and initial conditions be Equation 3.25 and 3.29 respectively.

The solutions to $\frac{\partial u}{\partial t} = 0$ and $\frac{\partial^2 u}{\partial x^2} = 0$ are

$$\begin{cases} a_0 = C_d \\ b_0 = C_u - \dfrac{\Delta C}{L}x \end{cases}. \tag{3.102}$$

Adding Equation 3.100 and 3.101 together and dividing by 2 gives

$$u = \bar{C} - \frac{\Delta C}{2L}x + \frac{1}{2}\left[L_t^{-1}\left(DL_{xx}u - Nu\right) + D^{-1}L_{xx}^{-1}\left(L_t u + Nu\right)\right], \tag{3.103}$$

where $\bar{C} = \frac{C_u + C_d}{2}$ is the average value for the upstream and downstream water heads.

Denote $u_0 = \frac{a_0 + b_0}{2}$ and the parametrized form of Equation 3.103 becomes

$$u = u_0 + \frac{\mu}{2}\left[L_t^{-1}\left(DL_{xx}u - Nu\right) + D^{-1}L_{xx}^{-1}\left(L_t u + Nu\right)\right], \tag{3.104}$$

where μ is the parameter for parametrization.

Thus u and Nu are decomposed as

$$u = \sum_{j=0}^{\infty} \mu^j u_j \tag{3.105}$$

and

$$Nu = r\frac{\partial u}{\partial x} = \sum_{j=0}^{\infty} \mu^j P_j, \tag{3.106}$$

where P_j are the Adomian polynomials.

Substituting Equation 3.105 and 3.106 into 3.104 gives

$$\begin{aligned}\sum_{j=0}^{\infty}\mu^j u_j = u_0 + \frac{\mu}{2}\Bigg\{ L_t^{-1}\left[D\frac{\partial^2}{\partial x^2}\left(\sum_{j=0}^{\infty}\mu^j u_j\right) - \sum_{j=0}^{\infty}\mu^j P_j\right] \\ + D^{-1}L_{xx}^{-1}\left[\frac{\partial}{\partial t}\left(\sum_{j=0}^{\infty}\mu^j u_j\right) + \sum_{j=0}^{\infty}\mu^j P_j\right]\Bigg\}.\end{aligned} \tag{3.107}$$

By comparing both sides of Equation 3.107, Equation 3.108 it can be obtained that (Cherruault, 1989; Cherruault et al., 1992)

$$\begin{cases} u_1 = \frac{1}{2}\left[L_t^{-1}\left(D\frac{\partial^2 u_0}{\partial x^2} - P_0\right) + D^{-1}L_{xx}^{-1}\left(\frac{\partial u_0}{\partial t} + P_0\right)\right] \\ u_2 = \frac{1}{2}\left[L_t^{-1}\left(D\frac{\partial^2 u_1}{\partial x^2} - P_1\right) + D^{-1}L_{xx}^{-1}\left(\frac{\partial u_1}{\partial t} + P_1\right)\right] \\ \ldots \\ u_{j+1} = \frac{1}{2}\left[L_t^{-1}\left(D\frac{\partial^2 u_j}{\partial x^2} - P_j\right) + D^{-1}L_{xx}^{-1}\left(\frac{\partial u_j}{\partial t} + P_j\right)\right] \end{cases}. \tag{3.108}$$

Subsitituting Equation 3.105 into 3.106 gives

$$Nu = \sum_{j=0}^{\infty}\mu^j P_j = r\frac{\partial u}{\partial x} = r\sum_{j=0}^{\infty}\mu^j u_j. \tag{3.109}$$

Since P_j can be expressed as $P_j = P_j\left(u_0, u_1, ..., u_j\right)$ when $r\,(x)$ is known, Equation 3.110 can be obtained:

$$\begin{cases} P_0 = r\,u_0 \\ P_1 = r\,u_1 \\ \ldots \\ P_j = r\,u_j \end{cases}. \tag{3.110}$$

Therefore by iteration, Equation 3.111 can be obtained:

$$\begin{cases} u_0 = \bar{C} - \dfrac{\Delta C}{2L}x = \dfrac{\Delta C}{2}\left(\widetilde{C} - \dfrac{x}{L}\right) \\ P_0 = \dfrac{r\Delta C}{2}\left(\widetilde{C} - \dfrac{x}{L}\right) \\ u_1 = \dfrac{\Delta C}{4}\left\{\left[r\left(\dfrac{x}{L} - \widetilde{C}\right)\right]t + \dfrac{1}{D}\left[\displaystyle\int_0^x \int_0^x r\left(\widetilde{C} - \dfrac{x}{L}\right)dxdx\right]\right\} \\ \cdots \end{cases}, \tag{3.111}$$

where $\widetilde{C} = \frac{2\bar{C}}{\Delta C} = \frac{C_u + C_d}{C_u - C_d}$.

When $C_d = 0$, Equation 3.111 becomes

$$\begin{cases} u_0 = 1 - \dfrac{C_u}{2L}x = \dfrac{C_u}{2}\left(1 - \dfrac{x}{L}\right) \\ P_0 = \dfrac{rC_u}{2}\left(1 - \dfrac{x}{L}\right) \\ u_1 = \dfrac{C_u}{4}\left\{\left[r\left(\dfrac{x}{L} - 1\right)\right]t + \dfrac{1}{D}\left[\displaystyle\int_0^x \int_0^x r\left(1 - \dfrac{x}{L}\right)dxdx\right]\right\} \\ \cdots \end{cases}. \tag{3.112}$$

In the u_1 equation in Equation 3.111 and 3.112, the integration for $r\left(\widetilde{C} - \frac{x}{L}\right)$ is non-elementary for the majority of the cross-sectional area function $A(x)$, and only few $A(x)$, such as $A(x) = e^x$ and $A(x) = kx + d$ $(kx + d > 0)$, can make u_1 and its following iterated equations be elementary. Therefore the ADM method is not efficient in solving the nonlinear governing equation as a semi-analytical method, and more techniques are required to supplement the method.

Chapter 4

Case study

4.1 Breakthrough time

The results of the normalized breakthrough time $\hat{t}_b$ under different Pe and $\widehat{\mathrm{MDR}}_{\mathrm{lim}}$ are plotted as diagrams in Figure B.1, B.2 and B.3, with examples to illustrate the application of the diagrams.

4.1.1 Breakthrough time diagrams

200 terms in series are applied in the calculation of Equation 3.78 and 3.82 by Matlab®. The logarithm of normalized breakthrough time versus the logarithm of Pe diagram is shown in Figure B.3, and it can be seen that when $\widehat{\mathrm{MDR}}_{\mathrm{lim}}$ is a fixed value, as Pe increases, $\hat{t}_b$ decreases, which indicates that the increase of advection process shall enhance the transportation of pullutant mass and reduce the normalized breakthrough time.

As Pe increases from 10 to 100, the curves tend to be linear, thus the curves are plotted as lines converging at $(500, 0.002)$ when Pe is larger than 100. Obviously Pe = 500 is the defined critical point to be large enough, and the subsequent diagram is shown in Figure B.1, where $\hat{t}_b = \frac{1}{\mathrm{Pe}}$ is plotted as a line in the logarithm of ordinate and abscissa. In the exact situation the curves will intersect at the infinity and be infinitely close to $\hat{t}_b = \frac{1}{\mathrm{Pe}}$ as Pe approches infinity.

In Figure B.3, when Pe is close to 1, $\hat{t}_b$ is tending to be steady, thus Pe = 1 is chosen to be the critical point for being small enough. When $\mathrm{Pe} \leqslant 1$, it is regarded that the varying of Pe does not affect $\hat{t}_b$ anymore and in Figure B.2 the red dash dot line represents this situation, where

other curves for different values of Pe are plotted as well in the $\widehat{\text{MDR}}_{\text{lim}}$ versus the logarithm of $\hat{t}_b$ chart. It is obvious that when $\widehat{\text{MDR}}_{\text{lim}}$ is extremely close to 0 and 1, the curves become steep. When $\widehat{\text{MDR}}_{\text{lim}} = 0$, $\hat{t}_b$ shall be 0, while when $\widehat{\text{MDR}}_{\text{lim}} = 1$, it shall take infinite time for the process to reach steady state.

4.1.2 Examples

Deploying Figure B.1, B.2 and B.3 shall give quick rough estimation of breakthrough time with various parameter values, or suggestions for parameter determination when the required breakthrough time is known.

Three examples are shown below to illustrate the application of the breakthrough time diagrams, and the necessary data are shown in Table 4.1. The soils in example 1, 2, 3 are the soil of standard quality waterproof curtain, highly-moderately weathered bedrock and silty clay respectively, which are referred from in Table 3.2, and the values of the hydraulic conductivity k, coefficient of diffusivity D_c and porosity n of the soils are also referred.

Table 4.1: Data for examples as illustration for the application of breakthrough time diagrams

Example	Hydraulic conductivity k unit: m/s	Waterhead difference ΔH unit : m	Coefficient of diffusivity D_c unit : m^2/s	Porosity n unit : %	Length L unit : m	Upstream contaminant concenctration C_u unit : mg/m^3	Cross-sectional area A unit : m^2	Contaminant mass discharge rate limit MDR_{lim} unit : mg/s
1	1.0×10^{-9}	1.2	2.0×10^{-10}	30	0.5	3.5×10^5	1.5	8.0×10^{-4}
2	2.8×10^{-5}	0.8	2.5×10^{-10}	20	-	2.0×10^5	-	-
3	1.4×10^{-6}	0	3.5×10^{-10}	41	3.0	1.5×10^5	-	1.0×10^{-5}

4.1.2.1 Example 1

It is known form Table 4.1 that Pe $= \frac{k\Delta H}{nD_c} = 20$, and $T = \frac{L^2}{D_c} = 1.25 \times 10^9$ s $= 39$ years. The steady downstream pollutant flux is $J_{sd} = 8.4 \times 10^{-4}$ mg/$\left(\text{m}^2 \cdot \text{s}\right)$, thus the normalized pollutant mass discharge rate is $\widehat{\text{MDR}}_{\text{lim}} = \frac{\text{MDR}_{\text{lim}}}{AJ_{sd}} = 0.63$. By linear interpolation it is known that the normalized breakthrough time $\hat{t}_b = \frac{0.054-0.044}{0.8-0.5} \times (0.63 - 0.5) + 0.044 = 0.048$ from Figure B.3. Therefore the breakthrough time $t_b = \hat{t}_b T = 1.9$ years. By Equation 3.70 the analytical result $\hat{t}_b$ is 0.048 as well, which agrees with the result by interpolation method with the diagrams.

4.1.2.2 Example 2

In example 2, Pe = $\frac{k\Delta H}{nD_c} = 4480$, and the breakthrough time should be $\hat{t}_b = \frac{1}{\text{Pe}} = 2.23 \times 10^{-4}$. If penetration happens, when the breakthrough time is required to be more than 30 years, the length of the process L should be more than 0.49 meters.

4.1.2.3 Example 3

Since $\Delta H = 0$ in example 3, Pe = 0, which indicates this is a pure diffusion scenario. The time base $T = \frac{L^2}{D_c} = 2.57 \times 10^{10}$ s = 815.4 years and the downstream pollutant flux is $J_{spd} = 7.2 \times 10^{-5}$ mg/$\left(\text{m}^2 \cdot \text{s}\right)$. When the required breakthrough time is 50 years, the normalized breakthrough time $\hat{t}_b = \frac{50}{815.4} = 0.0613$. From Figure B.2 it is known that $\widehat{\text{MDR}}_{\text{lim}} = 0.009$, and the maximum cross-sectional area is $A = \frac{\text{MDR}_{\text{lim}}}{\widehat{\text{MDR}}_{\text{lim}}} J_{spd} = 15.4\ \text{m}^2$.

4.2 Theoretical verification of the 1D FEM algorithm

Since Equation 3.28 can be solved analytically, it is possible to compare the results by the 1D FEM alogorithm (Schirén, 2018) with the theoretical solutions, which shares the same advection-diffusion governing equation. The verificaion in Schirén (2018) is not perfect, thus it is applied here to give another trial.

4.2.1 Parameter setup

There are 100 terms in series for the simulation of analytical normalized pollutant fluxes based on Equation 3.69, 3.70, 3.72 and 3.73 by Matlab®. To simplify the verification, the length of the path L is set to be 1 meter, the diffusion coefficient D_c is 5×10^{-10} m^2/s, and the characteristic time for normalization T is thus 8 billion seconds, which is approximately 253.7 years. The length L is discretized into 100 equal segments.

The steady seepage velocities for case verification is shown in Table 4.2.

Table 4.2: Steady seepage velocities for analytical verification

Case No.	**1**	**2**	**3**
Steady seepage velocity [m/s]	5×10^{-11}	5×10^{-10}	5×10^{-9}
Péclet number Pe	0.1	1	10

4.2.2 Results and interpreation

To facilitate the comparision between the theoretical and FEM results, the normalized pollutant fluxes for case 1, 2 and 3 are plotted in Figure 4.1, 4.2 and 4.3 respectively, where the normalized pollutant fluxes at the upstream inlet and downstream outlet are both included. Here the pollutant fluxes in the pure diffusion scenario are normalized based on the steady downstream pollutant flux in the advection-diffusion process to give an intuitive impression on the contribution of the advection process over the diffusion process in the transportation of the pollutant mass.

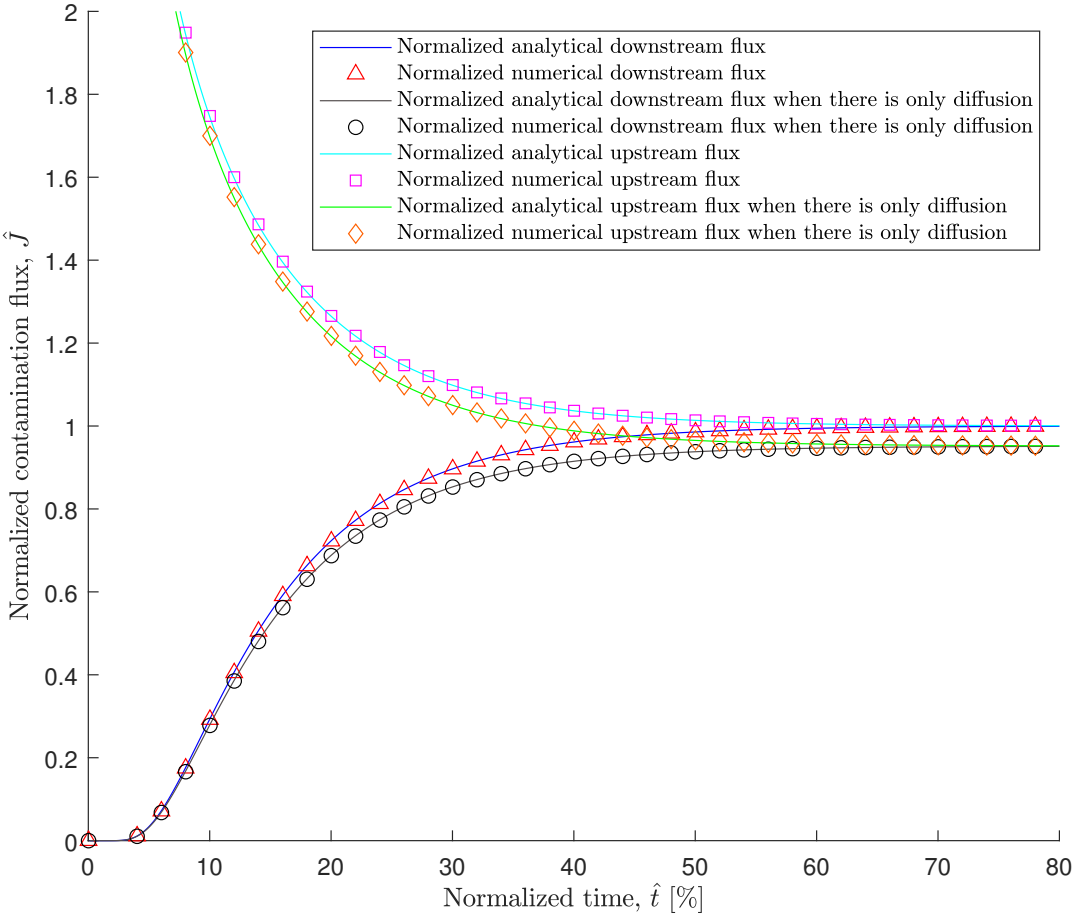

Figure 4.1: Plot for normalized pollutant flux in case 1

The analytical results agrees well with the FEM results, and in 3 cases all curves converges when

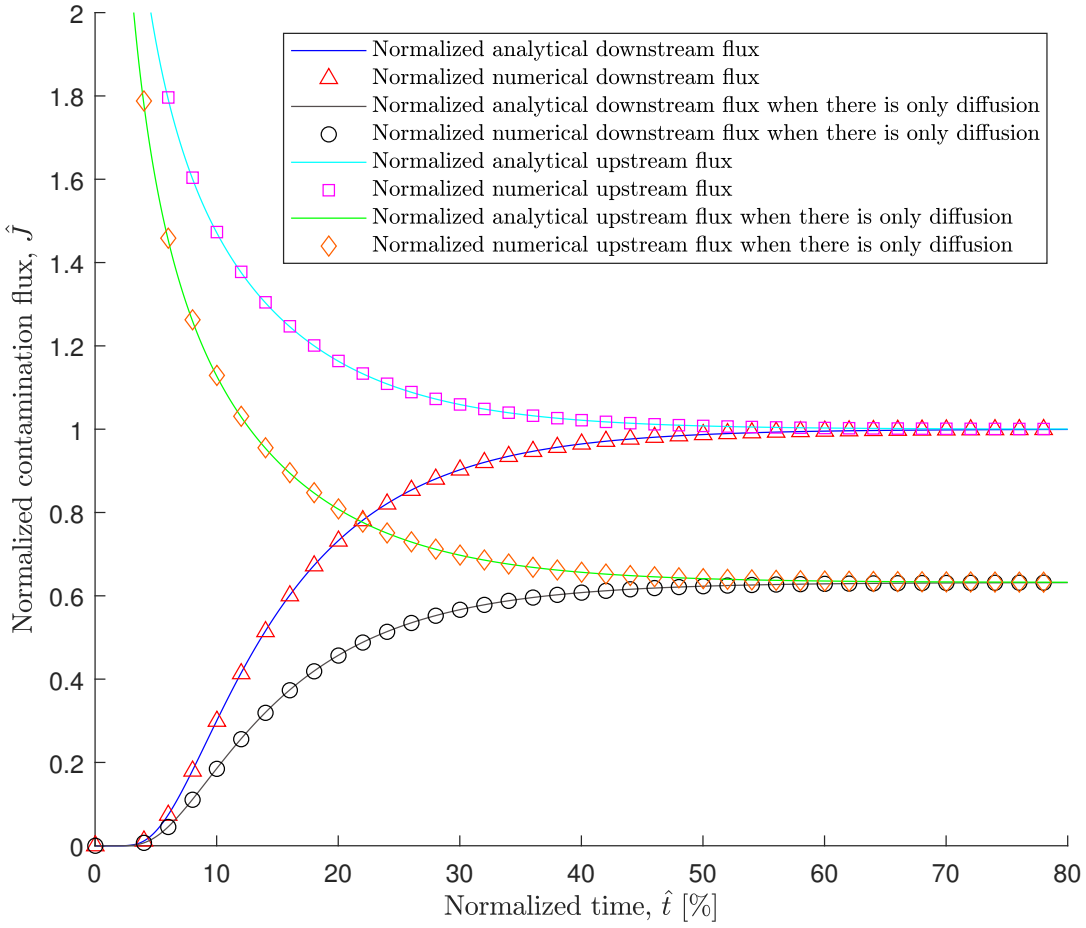

Figure 4.2: Plot for normalized pollutant flux in case 2

time is large enough, which verifies the conservation law of pollutant mass. The results for the pure diffusion scenario are the same in 3 cases.

When v_s is relatively small as 5×10^{-11} m/s in case 1 (Figure 4.1), the Péclet number is 0.1, and the diffusion process domains the advection-diffusion process, where the difference between the analytical and FEM results are negligible. It takes approximately 60% of T, i.e. 152.2 years for the process to be steady.

In Figure 4.2, it can be seen that when the steady seepage velocity is larger as 5×10^{-10} m/s, Pe = 1, and the advection process is no longer ignorable. The normalized upstream fluxes with the contribution of advection are smaller than those in pure diffusion scenario, while the nor-

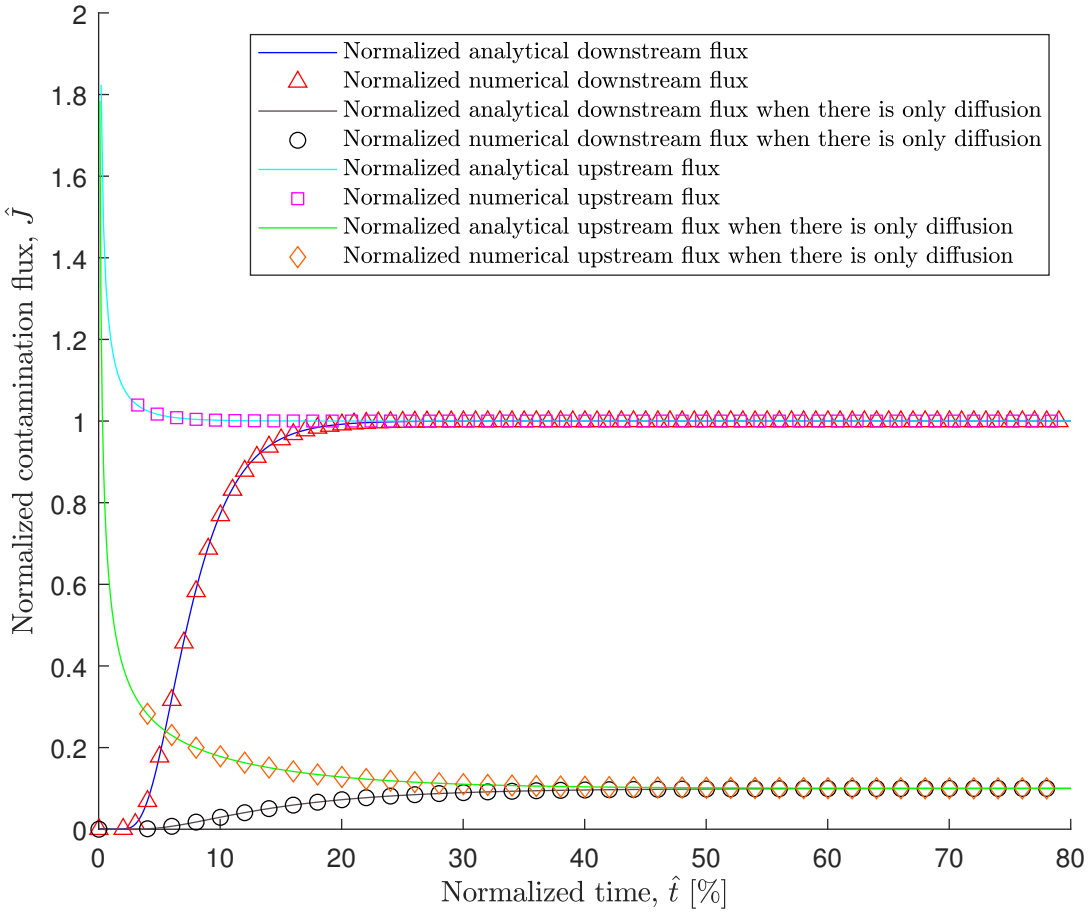

Figure 4.3: Plot for normalized pollutant flux in case 3

malized downstream fluxes are larger than the pure diffusion downstream fluxes. The shapes for the two downstream fluxes curves are simliar, and they are approximately synchronized regarding the same level of $\widehat{\text{MDR}}_{\text{lim}}$, which means for the same $\widehat{\text{MDR}}_{\text{lim}}$, the normalized breakthrough time are almost equal for the two downstream curves, and this verifies that when $\text{Pe} \leqslant 1$ it is reasonable to regard the advection-diffusion process as pure diffusion process for the calculation of normalized breakthrough time.

When the seepage velocity is as large as 5×10^{-9} m/s (Figure 4.3), the differences are significantly larger, which means the normalized fluxes for the advection-diffusion process are significantly larger than those for the pure diffusion process, and it takes much less time, i.e. approximately $25\%T$ for the fluxes with the contribution of advection to reach steady state than those without

the contribution of advection.

Chapter 5

Results and discussion

The definition and judge criterion for the breakthrough time in the scenario of cutoff walls with inhomogeneous Dirichlet boundary conditions are given, and the breakthrough time diagrams for the 1D linear steady seepage and transient contaminant advection-diffusion coupled process are given to serve as risk assessment tools for contaminant leakage problem.

The analytical solution for 1D linear steady seepage and transient contaminant advection-diffusion coupled process agrees well with the results by FEM for 3 cases with different Péclet numbers, which proves the validity of the FEM method.

When the pollutant concentration at the downstream is not zero, the equations for the pollutant flux and the breakthrough time need to be modified.

As the nonlinear model is given, the FEM algorithm shall be modified to include the nonconstant cross-sections and be compared with the given FDM algorithm. The model shall be combined with the TDA 3D model for JGCOW and diaphragm wall or other models for defective cutoff walls to evaluate the contaminant mass discharge rate. The breakthrough time for nonlinear situations can thus be determined with the given definition and judge criterion, and the analogical breakthrough time diagrams shall be plotted to function as tools for the contaminant leakage risk assessment regarding cutoff walls with construction errors.

Although the ADM algorithm for the nonlinear model is given, it is only feasible for few types of

1D channels, therefore an improvement shall be applied for the ADM algorithm.

The development of the nonlinear model and the breakthrough time as a risk assessment criterion is consistent with the aim of the thesis, which is to evaluate the pollutant mass discharge rate in cutoff walls with random construction errors. Since the time is limited, the parametric study for the integration of the nonlinear model with stochastically defective cutoff wall simulations is not performed in the thesis.

Chapter 6

Conclusion and future perspectives

The summary and conclusion for the results of the works by the thesis are listed:

1. The breakthrough time diagrams are plotted as contaminant leakage risk assessment tools and the model with its FDM and ADM algorithms regarding 1D nonlinear steady seepage and transient contaminant advection-diffusion coupled process are proposed.
2. In linear scenarios, the analytical solution and FEM algorithm shall be valid as they verify each other.
3. Since the definition and judge criterion for contaminant breakthrough time of defective cutoff walls can be applied in the nonlinear scenarios as well, the combination of the nonlinear model with 2D and 3D simulations of cutoff walls with construction errors shall be a realistic and promising way to perform contaminant leakage risk assessment.

The recommendations for future study are listed as short-term, medium-term and long-term recommendations:

- Short-term: The nonlinear steady seepage and transient contaminant advection-diffusion coupled model shall be integrated with the TDA stochastic 3D model or other models for defective cutoff walls to assess the contaminant leakage risk by determining the breakthrough time and plot the breakthrough time diagrams. The definition of Péclet number in nonlinear scenario shall be studied to obtain a profound understand regarding the process. Other numerical methods, e.g. FEM method and lattice Boltzmann method shall be applied to solve the model and be compared with the given FDM method.

- Medium-term: In the thesis, only the value of the varying cross-sectional area and the cross-sectionally average seepage velocity is considered, while the shape of the cross-section and the tortuousness of the path for the process shall influence the motion of groundwater together with the contaminants in the groundwater. Thus it is necessary to develop more realistic models and algorithms to describe the process.
- Long-term: Fractal geometry can be applied to simulate complex channels, which can be combined with the seepage and contaminant advection-diffusion coupled process to simulate the groundwater flow and contaminant transportation in medium with complex channels.

.

Appendix A

Acronyms

1D One Dimensional

2D Two Dimensional

3D Three Dimensional

ADM Adomian Decomposition Method

CEC Contaminants of Emerging Concern

CGCW Composite Geomembrane Cut-off Wall

COD Chemical Oxygen Demand

COV Coefficient of Variation

FDM Finite Difference Method

FEM Finite Element Method

GCL Geosynthetic Clay Liner

IID Independently Identically Distribution

JGCOW Jet-Grouted Cut-Off Wall

MSW Municipal Solid Waste

ODE Ordinary Differential Equation

PBFC Polyvinyl Alcohol-Bentonite-Fly ash-Cement

RFEM Random Finite Element Method

SHMP Sand/Sodium Hexametaphosphate (SHMP)

SB Soil-bentonite

SPSP Steel Pipe Sheet Pipe

TDA Three-Dimensional Discretized Algorithm

Appendix B

Breakthrough time diagrams

B.1 Pe as abscissa (Pe $\geqslant$ 500)

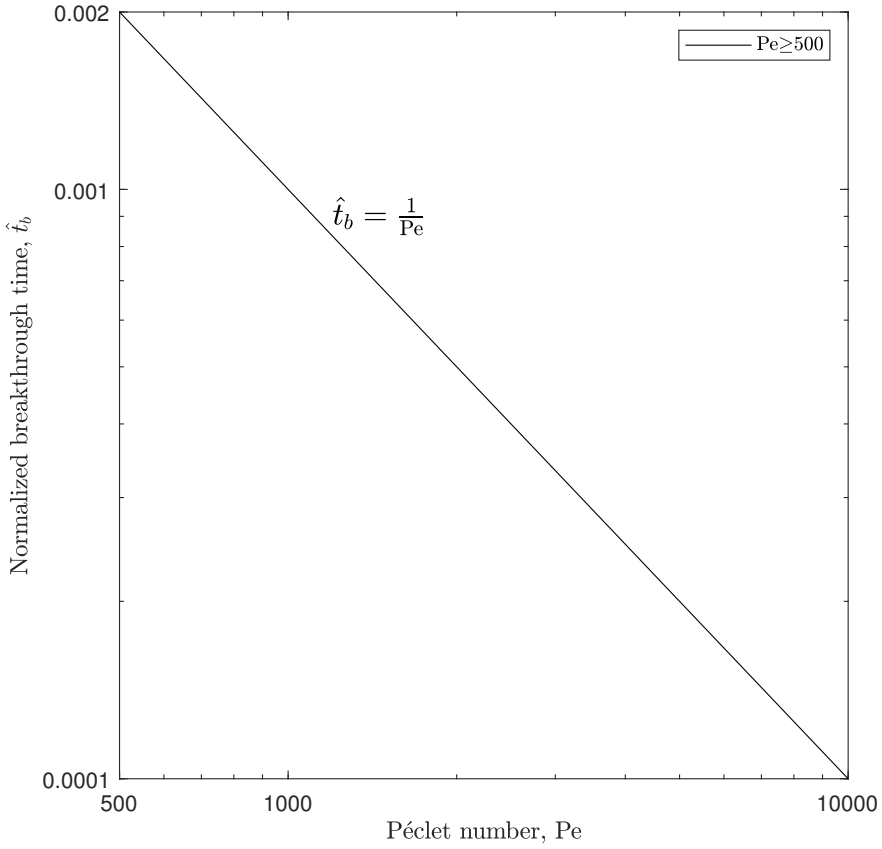

Figure B.1: Diagram of normalized breakthrough time $\hat{t}_b$ versus Péclet number Pe when Pe$\geqslant$500

B.2 $\widehat{\text{MDR}}_{\text{lim}}$ as abscissa $\left(0.1\% \leqslant \widehat{\text{MDR}}_{\text{lim}} \leqslant 99.9\%\right)$

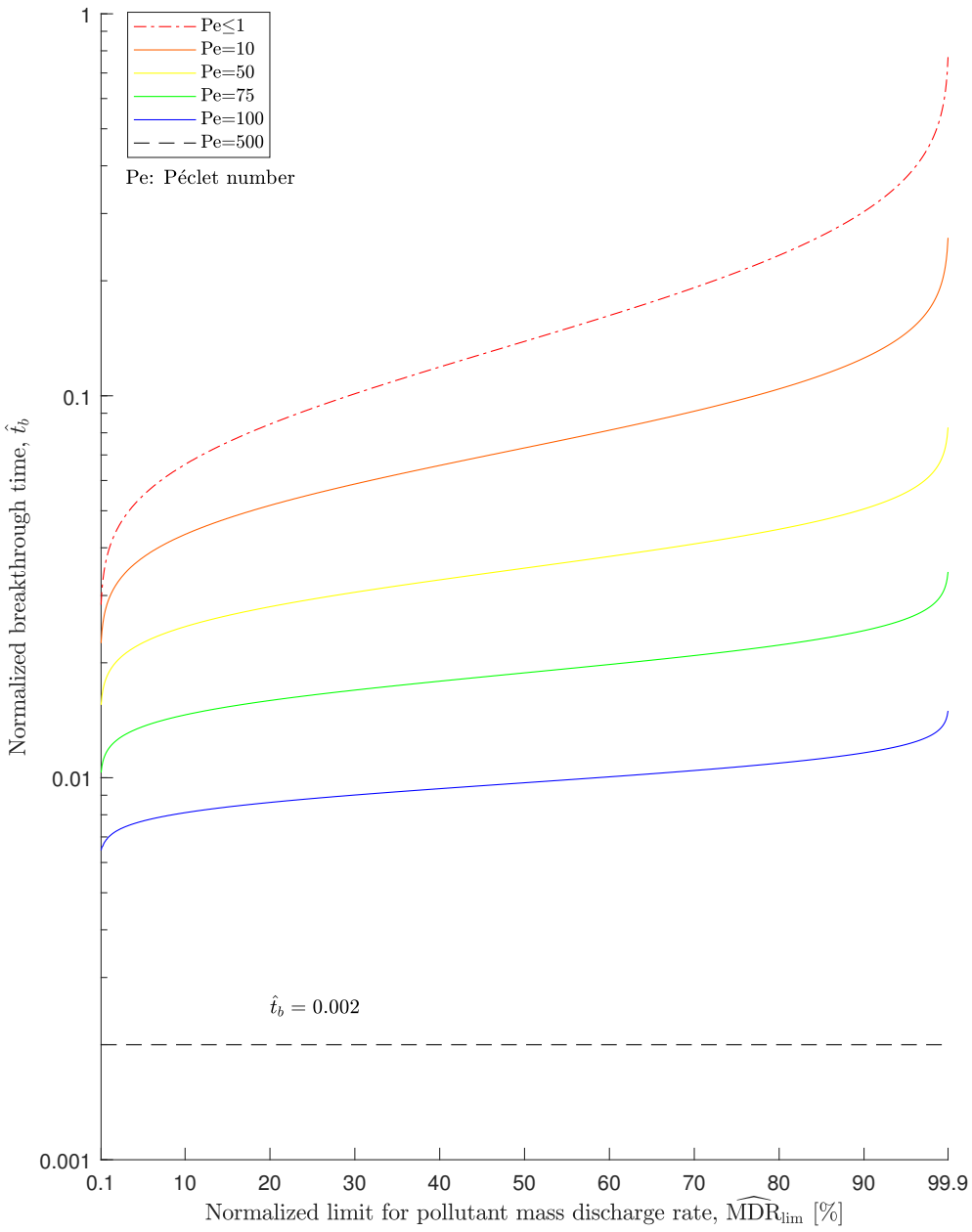

Figure B.2: Diagram of normalized breakthrough time $\hat{t}_b$ versus normalized limit for pollutant mass discharge rate $\widehat{\text{MDR}}_{\text{lim}}$ when $0.1\% \leqslant \widehat{\text{MDR}}_{\text{lim}} \leqslant 99.9\%$

B.3 Pe as abscissa (1 < Pe < 500)

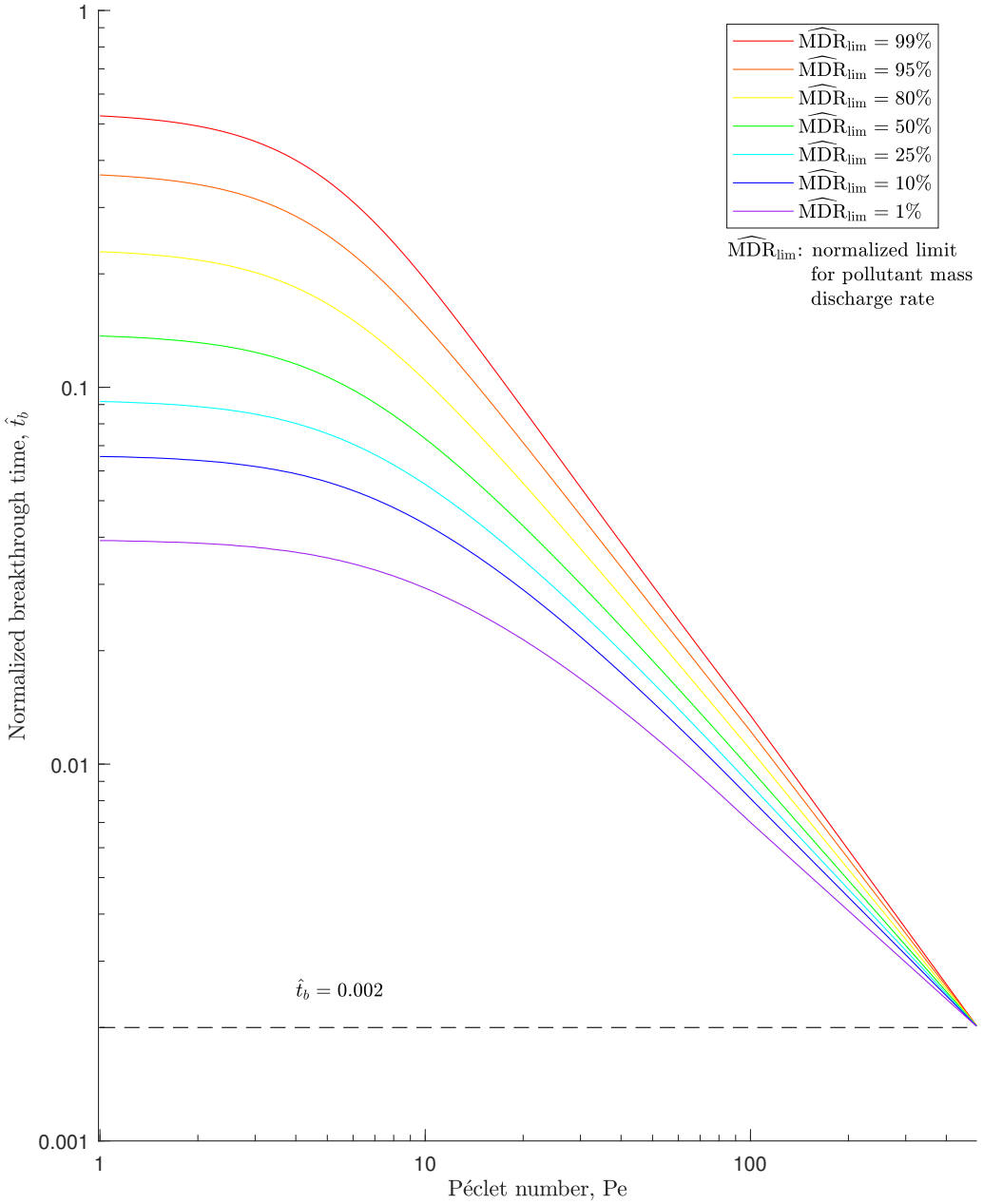

Figure B.3: Diagram of normalized breakthrough time $\hat{t}_b$ versus Péclet number Pe when 1<Pe<500

Bibliography

Abu-Rukah, Y. and Al-Kofahi, O. (2001). The assessment of the effect of landfill leachate on ground-water quality—a case study. el-akader landfill site—north jordan. *Journal of Arid Environments*, 49(3):615–630.

Adamo, N., Al-Ansari, N., Sissakian, V., Laue, J., and Knutsson, S. (2020). Dam safety problems related to seepage. 10:191–239.

Adomian, G. (1984). A new approach to nonlinear partial differential equations. *J. Math. Anal. Appl.*

Adomian, G. (1986a). Application of the decomposition method to the navier-stokes equations. *J. Math. Anal. Appl.*

Adomian, G. (1986b). *Nonlinear Stochastic Operator Equations*. Academic Press.

Adomian, G. (1988). A review of the decomposition method in applied mathematics. *J. Math. Anal.Appl.*

Adomian, G. (1989). *Nonlinear Stochastic Systems Theory and Applications to Physics*. Kluwer Academic Publishers.

Adomian, G. (1994). *Solving frontier problems of physics: the decomposition method*. Kluwer Acad. Publ.

Adomian, G. (1997). Explicit solutions of nonlinear partial differential equations. *Appl. Math. Comput.*

Amos, P., Bruce, D., Lucchi, M., Watkins, N., and Wharmby, N. (2020). Design and construction of deep secant pile seepage cut-off walls under the Arapuni dam in New Zealand.

Arroyo, M., Gens, A., Croce, P., and Modoni, G. (2012). *Design of jet-grouting for tunnel waterproofing*, page 181–188. CRC Press/Balkema.

Brown, J. W. and Churchill, R. V. (1993). *Fourier Series and Boundary Value Problems*. Mcgraw-Hill College, 5 edition.

Castaldo, P., Jalayer, F., and Palazzo, B. (2018). Probabilistic assessment of groundwater leakage in diaphragm wall joints for deep excavations. *Tunnelling and Underground Space Technology*, 71:531–543.

Chen, Y., Wang, Y., and Xie, H. (2015). Breakthrough time-based design of landfill composite liners. *Geotextiles and Geomembranes*, 43(2):196–206.

Cheng, S.-H., Liao, H.-J., Yamazaki, J., Wong, R., and Iwakubo, T. (2020). Alignment of vertical and inclined jet grout columns for waterproofing. *Geotechnical Testing Journal*, 43:20180324.

Cheng, W.-C., Li, G., Zhou, A., and Xu, J. (2019). Rethinking the water leak incident of tunnel luo09 to prepare for a challenging future. *Advances in Civil Engineering*, 2019.

Cherruault, Y. (1989). Convergence of adomian's method. *Kybernetes*, 18(2):31–38.

Cherruault, Y., Saccomandi, G., and Some, B. (1992). New results for convergence of adomian's method applied to integral equations. *Mathematical and Computer Modelling*, 16(2):85–93.

Conway, B. D. (2016). Land subsidence and earth fissures in south-central and southern Arizona, USA. *Hydrogeology Journal*, 24(3):649–655.

Croce, P., Flora, A., and Modoni, G. (2004). *Jet grouting. Tecnica, progetto e controllo*.

Croce, P. and Modoni, G. (2007). Design of jet-grouting cut-offs. *Proceedings of the Institution of Civil Engineers - Ground Improvement*, 11(1):11–19.

Dai, G., Zhu, J., Song, Y., Li, S., and Shi, G. (2020). Experimental study on the deformation of a cut-off wall in a landfill. *KSCE Journal of Civil Engineering*, 24(5):1439–1447.

De Wit, J., Bogaards, P., Langhorst, O., Schat, B., Essler, R., Maertens, J., Obladen, B., Bosma, C., Sleuwaegen, J., and Dekker, H. (2007). Design and validation of jetgrouting for the central station amsterdam. In *Geotechniek, SpecialNumber on Madrid XIV European Conference of Soil Mechanics and Foundation Engineering*.

Devlin, J. F. and Parker, B. L. (1996). Optimum hydraulic conductivity to limit contaminant flux through cutoff walls. *Groundwater*, 34(4):719–726.

Ding, X.-H., Feng, S.-J., Zheng, Q.-T., and Peng, C.-H. (2020). A two-dimensional analytical model for organic contaminants transport in a transition layer-cutoff wall-aquifer system. *Computers and Geotechnics*, 128:103816.

Du, Y.-J., Fan, R.-D., Reddy, K. R., Liu, S.-Y., and Yang, Y.-L. (2015). Impacts of presence of lead contamination in clayey soil–calcium bentonite cutoff wall backfills. *Applied Clay Science*, 108:111–122.

Eramo, N., Modoni, G., and Arroyo, M. (2012). *Design control and monitoring of a jet grouted excavation bottom plug*, page 611–618. CRC Press/Balkema.

Evans, J. C. and Ruffing, D. G. (2017). *Design and Construction of an Experimental Soil-Bentonite Cutoff Wall*, pages 164–174.

Fatta, D., Papadopoulos, A., and Loizidou, M. (1999). A study on the landfill leachate and its impact on the groundwater quality of the greater area. *Environmental Geochemistry and Health*, 21(2):175–190.

Feng, S.-J., Zhao, Y., Zhang, X.-L., and Bai, Z.-B. (2020). Leachate leakage investigation, assessment and engineering countermeasures for tunneling underneath a msw landfill. *Engineering Geology*, 265:105447.

Flora, A., Lirer, S., Lignola, G. P., and Modoni, G. (2012). Mechanical analysis of jet grouted supporting structures. In Viggiani, G., editor, *Geotechnical Aspects of Underground Construction in Soft Ground*, pages 819–828. CRC Press.

Flora, A., Modoni, G., Lirer, S., and Croce, P. (2013). The diameter of single, double and triple fluid jet grouting columns: Prediction method and field trial results. *Géotechnique*, 63:934–945.

Fu, X.-L., Zhang, R., Reddy, K. R., Li, Y.-C., Yang, Y.-L., and Du, Y.-J. (2021). Membrane behavior and diffusion properties of sand/shmp-amended bentonite vertical cutoff wall backfill exposed to lead contamination. *Engineering Geology*, 284:106037.

Groundwater Engineering Limited. Cut off walls. https://www.groundwatereng.com/groundwater-control/cut-off-walls.

Guerrero, J., Pimentel, L. C., Skaggs, T., and Van Genuchten, M. (2009). Analytical solution of the advection-diffusion transport equation using a change-of-variable and integral transform technique. *International Journal of Heat and Mass Transfer*, 52:3297–3304.

Hekmatzadeh, A. A., Adel, A., Zarei, F., and Torabi Haghighi, A. (2019). Probabilistic simulation of advection-reaction-dispersion equation using random lattice boltzmann method. *International Journal of Heat and Mass Transfer*, 144:118647.

Ho, C.-E. (2007). Fluid-soil interaction model for jet grouting. pages 1–10.

Hong, C. S., Shackelford, C. D., and Malusis, M. A. (2017). Numerical evaluation of vertical cut-off walls comprising zeolite-amended backfills for enhanced metals containment. *Journal of Geotechnical and Geoenvironmental Engineering*, 143(7):04017028.

Hwang, W.-K., Kim, H.-E., Choi, H., and Kim, T.-H. (2019). Proper regulation of the cutoff system in offshore landfill built on clay ground with double walls. *Journal of the Korean Geotechnical Society*, 35(8):5–15.

Inazumi, S., Ohtsu, H., Otake, Y., Kimura, M., and Kamon, M. (2009). Evaluation of environmental feasibility of steel pipe sheet pile cutoff wall at coastal landfill sites. *Journal of Material Cycles and Waste Management*, 11.

Inazumi, S., Sekitani, M., Chae, K.-S., and Shishido, K.-I. (2017). Evaluation of maintenance strategies based on leakage risk assessment on side impervious walls at coastal landfill sites. *Materials Sciences and Applications*, 8(6):448–475.

Jacobi, C. G. J. (1829). *Fundamenta nova theoriae functionum ellipticarum*.

Koda, E. and Osinski, P. (2017). Bentonite cut-off walls: solution for landfill remedial works. *Environmental Geotechnics*, 4(4):223–232.

Koh, Y.-I. (2018). The study on cutting-off the leachate leakage or infiltration from waste landfill by wall mass constructed in underground. *Journal of the Korean GEO-environmental Society*, 19(10):27–34.

Lambe, T. W. and Whitman, R. V. (1969). *Soil mechanics*. Wiley, New York.

Lee, J.-Y., Choi, Y.-K., Kim, H.-S., and Yun, S.-T. (2005). Hydrologic characteristics of a large rockfill dam: Implications for water leakage. *Engineering Geology*, 80(1):43–59.

Liu, T., Sun, W., Kou, H., Yang, Z., Meng, Q., Zheng, Y., Wang, H., and Yang, X. (2019). Experimental study of leakage monitoring of diaphragm walls based on distributed optical fiber temperature measurement technology. *Sensors*, 19(10).

Liu, X.-X., Shen, S.-L., Xu, Y.-S., and Yin, Z.-Y. (2018). Analytical approach for time-dependent groundwater inflow into shield tunnel face in confined aquifer. *International Journal for Numerical and Analytical Methods in Geomechanics*, 42(4):655–673.

Mamaloukas, C. (2000). An approximate solution of burgers equation using adomian's decomposition method. In *Proceedings of the Conference of Applied Differential Geometry—General Relativity and the Workshop on Global Analysis, Differential Geometry and Lie Algebra*.

Modoni, G., Croce, P., and Mongiovì, L. (2006). Theoretical modelling of jet grouting. *Geotechnique*, 56:335–347.

Modoni, G., Flora, A., Lirer, S., Ochmański, M., and Croce, P. (2016). Design of jet grouted excavation bottom plugs. *Journal of Geotechnical and Geoenvironmental Engineering*, 142:04016018.

Mojtabi, A. and Deville, M. (2015). One-dimensional linear advection–diffusion equation: Analytical and finite element solutions. *Computers and Fluids*, 107:189–195.

Naveen, B. P., Sumalatha, J., and Malik, R. K. (2018). A study on contamination of ground and surface water bodies by leachate leakage from a landfll in bangalore, india. *International Journal of Geo-Engineering*, 9(1):27.

Pan, Y. and Fu, Y. (2019). Effect of random geometric imperfections on the water-tightness of diaphragm wall. *Journal of Hydrology*, 580:124252.

Pan, Y., Hicks, M. A., and Broere, W. (2021). An efficient transient-state algorithm for evaluation of leakage through defective cutoff walls. *International Journal for Numerical and Analytical Methods in Geomechanics*, 45(1):108–131.

Pan, Y., Liu, Y., and Chen, E. J. (2019a). Probabilistic investigation on defective jet-grouted cutoff wall with random geometric imperfections. *Géotechnique*, 69(5):420–433.

Pan, Y., Liu, Y., Hu, J., Sun, M., and Wang, W. (2017). Probabilistic investigations on the water-tightness of jet-grouted ground considering geometric imperfections in diameter and position. *Canadian Geotechnical Journal*, 54(10):1447–1459.

Pan, Y., Yi, J., Goh, S.-H., Hu, J., Wang, W., and Liu, Y. (2019b). A three-dimensional algorithm for estimating water-tightness of cement- treated ground with geometric imperfections. *Computers and Geotechnics*, 115.

Peng, C.-H., Feng, S.-J., Zheng, Q.-T., Ding, X.-H., Chen, Z.-L., and Chen, H.-X. (2020). A two-dimensional analytical solution for organic contaminant diffusion through a composite geomembrane cut-off wall and an aquifer. *Computers and Geotechnics*, 119:103361.

Phoon, K.-K. and Kulhawy, F. H. (1999). Characterization of geotechnical variability. *Canadian Geotechnical Journal*, 36(4):612–624.

Pujades, E., Carrera, J., Vázquez-Suñé, E., Jurado, A., Vilarrasa, V., and Mascuñano-Salvador, E. (2012). Hydraulic characterization of diaphragm walls for cut and cover tunnelling. *Engineering Geology*, 125:1 – 10.

Pujades, E., Jurado, A., Carrera, J., Vázquez-Suñé, E., and Dassargues, A. (2016). Hydrogeological assessment of non-linear underground enclosures. *Engineering Geology*, 207:91 – 102.

Qi, C., Huang, J., Wang, B., Deng, S., Wang, Y., and Yu, G. (2018). Contaminants of emerging concern in landfill leachate in china: A review. *Emerging Contaminants*, 4(1):1–10.

Ratiat, A., Khettal, T., and Meddi, M. (2020). The piezometric and isotopic analysis of leaks in earth dams: the case of the fountain of gazelle dam, biskra, algeria. *Environ Earth Sci*, 79(6):138.

Rowe, R. K. and Abdelatty, K. (2013). Leakage and contaminant transport through a single hole in the geomembrane component of a composite liner. *Journal of Geotechnical and Geoenvironmental Engineering*, 139(3):357–366.

Schirén, W. (2018). Finite element method for 1d transient convective heat transfer problems.

Sembenelli, P. (2016). *A Case of Piping in Sand Under a Dam and Its Back Analysis*, pages 311–336. Springer India, New Delhi.

Sembenelli, P. G. and Sembenelli, G. (1999). Deep jet-grouted cut-offs in riverine alluvia for Ertan cofferdams. *Journal of Geotechnical and Geoenvironmental Engineering*, 125(2):142–153.

Shen, S.-L., Wang, Z.-F., Yang, J., and Ho, C.-E. (2013). Generalized approach for prediction of jet grout column diameter. *Journal of Geotechnical and Geoenvironmental Engineering*, 139:2060–2069.

Shin, J., Lee, I., Lee, Y., and Shin, H. (2006). Lessons from serial tunnel collapses during construction of the seoul subway line 5. *Tunnelling and Underground Space Technology*, 21(3):296–297. Safety in the Underground Space - Proceedings of the ITA-AITES 2006 World Tunnel Congress and 32nd ITA General Assembly.

Shishido, K.-i. and Inazumi, S. (2019). Assessment on leakage risk of side impervious walls at coastal landfill sites. *International Journal of GEOMATE*, 16(54):86–93.

Tan, Y. and Lu, Y. (2017). Forensic diagnosis of a leaking accident during excavation. *Journal of Performance of Constructed Facilities*, 31(5):04017061.

Tyagi, A., Zulkefli, M., Pan, Y., Goh, S.-H., and Lee, F.-H. (2017). Failure modes of tunnels with improved soil surrounds. *Journal of Geotechnical and Geoenvironmental Engineering*, 143.

U.S. EPA (1978). In-depth studies on health and environmental impacts of selected water pollutants. Technical report, U.S. Environmental Protection Agency.

Wang, K., Li, Z., Zheng, H., Xu, X., and He, H. (2021). A theoretical model for estimating the water-tightness of jet-grouted cut-off walls with geometric imperfections. *Computers and Geotechnics*, 138:104316.

Wang, Y., Chen, Y., Xie, H., Zhang, C., and Zhan, L. (2016). Lead adsorption and transport in loess-amended soil-bentonite cut-off wall. *Engineering Geology*, 215:69–80.

Whittaker, E. T. and Watson, G. N. (1962). *A Course of Modern Analysis*. Cambridge University Press, 4th edition edition.

Wu, Y.-X., Shen, S.-L., Xu, Y.-S., and Yin, Z.-Y. (2015a). Characteristics of groundwater seepage with cut-off wall in gravel aquifer. i: Field observations. *Canadian Geotechnical Journal*, 52(10):1526–1538.

Wu, Y. X., Shen, S. L., Yin, Z. Y., and Xu, Y. S. (2015b). Characteristics of groundwater seepage with cut-off wall in gravel aquifer. ii: Numerical analysis. *Canadian Geotechnical Journal*, 52(10):1539–1549.

Xu, H., Shu, S., Wang, S., Zhou, A., Jiang, P., Zhu, W., Fan, X., and Chen, L. (2019). Studies on the chemical compatibility of soil-bentonite cut-off walls for landfills. *Journal of Environmental Management*, 237:155–162.

Zhan, L.-t., Liu, W., Zeng, X., and Chen, Y.-m. (2013). Parametric study on breakthrough time of vertical cutoff wall for msw landfills and simplified design formula for wall thickness. *Chinese Journal of Geotechnical Engineering*, 35(11):1988–1996.